IJES *Iranian Journal of Earth Sciences*
Vol. 12, No. 1, 2020, 10-31.

Study of micro-textures and chemistry of feldspar minerals of East Sarbisheh volcanic complex (Eastern Iran), for evidence of magma chamber process

Mahboobeh Jamshidibadr[*1], Sahar Tarabi[2], Kazem Gholizadeh[3]

1. Geology Department, Payame Noor University, 19395-4697 Tehran, Iran
2. Young Researchers and Elites club, Science and Research Branch, Islamic Azad University, Tehran, Iran
3. Iran minerals processing research center (IMPRC), Karaj, Iran

Received 15 April 2019; accepted 22 August 2019

Abstract

The Eocene-Oligocene Sarbisheh volcanic complex is a part of the Lut-Sistan Zone that outcrops in eastern Iran. In the east of this complex, three groups of volcanic rocks (i.e., andesite, dacite, and rhyolite) exist. Plagioclase as the main mineral of these rocks is found with varying micro-textures. Based on a changing trend in the concentration of anorthite, the developed micro-textures (coarse/fine-sieve, fine-scale oscillatory zoning, and resorption surfaces) are not affected by the chemical composition of the magma. Rather, such changes can occur by temperature variations during magma crystallization or H_2O fugacity changes in the magmatic system. The recharge of basic magma leads to a temperature rise, partial melting of the central part of the crystal, and formation of sieve texture, and resorption surfaces. Consequently, the chemical changes of magma in the chamber cause the formation of An-enrichment in the outer layer of the plagioclase crystal and formation of oscillatory zoning. In addition, the morphological micro-textures (i.e., glomerocryst, synneusis, swallow-tailed, microlite, and broken crystals) are developed by the influence of dynamic behavior of the crystallizing magma and magmatic differentiation. The thermobarometry evaluation using pyroxene and biotite chemistry showed that the temperature ranges between 700 and 1150°C and the pressure were less than 2 kbar.

Keywords: *Plagioclase, Micro-textures, Magma, Sarbisheh Volcanic Complex, Lut-Sistan Zone*

1. Introduction

The Eocene-Oligocene magmatic erupt is important event in the magmatic evidence of Iran follow-on in common magmatic rocks through the country (Figs 1a,1b) (Schroder 1944; Verdel et al. 2011). These magmatic rocks of Iran are mainly seen in the Lut-Sistan region, eastern Iran, around Urumieh-Dokhtar magmatic arc (UDMA) in southwestern Iran, and the Alborz ranges in northern Iran. In this research, we focus on the magmatic rocks in Lut-Sistan region.

The Sistan suture zone, eastern Iran, is N-S-trending branch of Neotethys with a complex tectonic history (McCall 1997; Camp and Griffis 1982; Tirrul et al. 1983). Based on the radiolarian records, the Sistan Ocean was opened by the Early Cretaceous (Babazadeh and deWever 2004). Base on dating from the leucogabbros (Birjand ophiolite) that reported by Zarrinkoub et al. (2012) shows that the generation of oceanic lithosphere was until active in the Middle Cretaceous. In this regard, the timing and mechanism of ocean closure are not wholly understood. For instance, models involving eastward subduction under the Afghan block, western subduction under the Lut block, two-sided subduction, and eastward intra-oceanic subduction have been suggested (Camp and Griffis 1982; Tirrul et al. 1983; Arjmandzadeh et al. 2011; Zarrinkoub et al. 2012).

The age for ocean closure and thus the Lut-Afghan collision were considered by some researchers to take place in the Middle Eocene (Camp and Griffis 1982; Tirrul et al. 1983). Some others, however, attribute it to the Late Cretaceous (Zarrinkoub et al. 2012; Angiboust et al. 2013). Based on dating reported by Bröcker et al. (2013) the subduction was active in the Late Cretaceous. Sarbisheh volcanic complex (SVC) is situated 15 km northeast of Sarbisheh in South Khorasan province, Iran. This complex is located between the longitude 59° 49′ 52″ to 60° E and latitude 32° 34′ 28″ to 32° 43′ 25″ N (Fig 1c). Also, based on the structural classification of Iran, this region is situated in Sistan zone (Camp and Griffis 1982; Tirrul et al. 1983; Karimpour et al. 2011; Karimpour et al. 2012; Pang et al. 2012; Pang et al. 2013). Previous studies aimed at investigating the whole rock chemistry of intrusive and volcanic masses, as well as their isotopic results considering the petrogenetic properties using the evaluation of ophiolites and finally presented a tectonic model for Lut-Sistan region (Bröcker et al. 2013).

In the east of SVC, andesite and dacite rocks contain plagioclase minerals with various micro-textures, which can be used to identify and evaluate the micro-texture morphology and mineralogy. Therefore, in the present study, the volcanic rocks of East-SVC were described in terms of micro-texture morphology and their formation mechanism was discussed.

*Corresponding author.
E-mail address (es): m_jamshidi@pnu.ac.ir

Since the plagioclase is one of the main minerals in magmatic crystallization, the study of the micro-texture morphology of plagioclases and their chemistry can provide valuable information about magmatic crystallization process (Pietranik et al. 2006; Kahl et al. 2015; Viccaro et al. 2015; Yazdi et al. 2017). Besides, many researchers have performed studies on the zoning of plagioclases to determine the magmatic crystallization process (e.g., Waight et al. 2000; Ginibre et al. 2002; Karsli et al. 2004; Vernon 2004, Pietranik et al. 2006; Ginibre et al. 2007 ; Smith et al. 2009). In the present research, mineralogical study, evaluation of mineral chemistry, the introduction of micro-textures of plagioclases, and thermobarometry were conducted and a final model was presented to show the condition of crystallization in the magmatic chamber and the way of forming micro-textures of plagioclases.

2. Geology background

The Lut-Sistan region (~31 to 35° N and ~57 to 61° E) is a place with abundant Eocene-Oligocene magmatic rocks outcrops in the eastern Iran areas (Karimpour et al. 2011). These rocks cover an area of ~300 km × 400 km, based on existing outcrops, which is a least approximation because their exposure might even expand to western Afghanistan. In contrast, the east Iranian magmatism appeared to have a diffuse pattern, with coeval magmatism elsewhere in Iran, forming linear or curved magmatic belts (e.g., UDMA and Alborz ranges), (Figs 1a, 1b). The eastern limit of magmatism is compared with the northern Sistan suture zone, while the western limit is demonstrates by the Nayband fault, an N-S-trending dextral strike-slip fault that is active in the Late Cenozoic (Walker and Jackson 2002; Walker et al. 2009). This fault also highlights the boundary between the Lut and Tabas blocks (Figs 1a,1b).

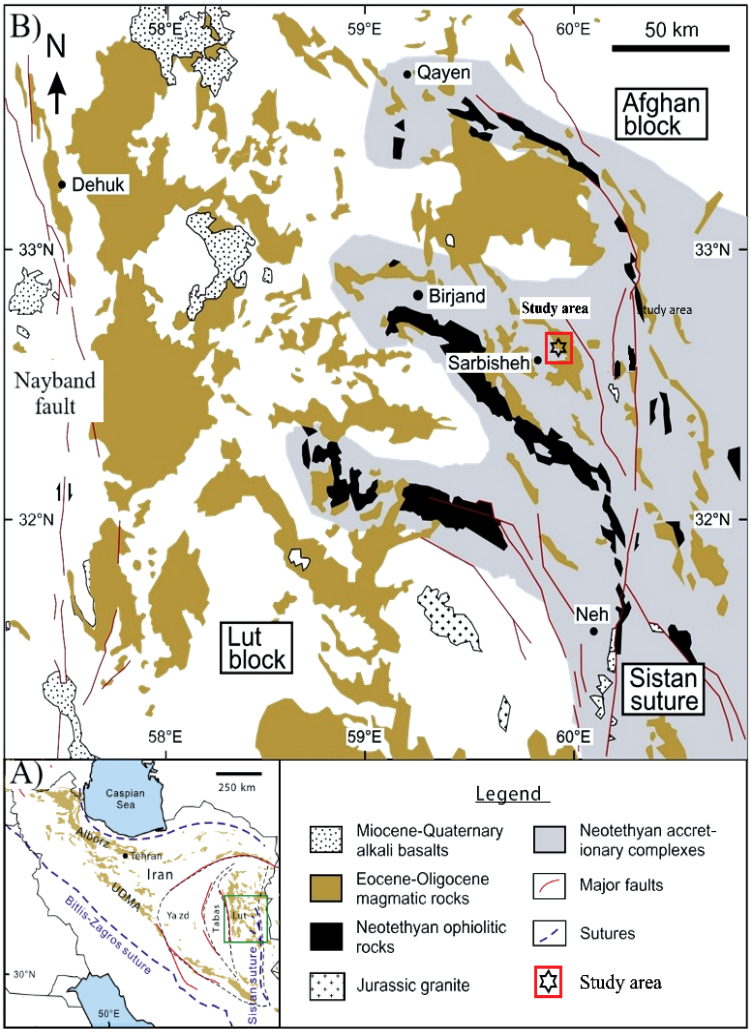

Fig 1. a. Location of Lut–Sistan Zone in the eastern Iran, b. Geological sketch map showing the study locations in the Lut–Sistan Zone (modified from Pang et al. 2012), c. A part of geological map of the East-SVC after the Sarbisheh 1:100000 geological map (Nazari and Salamati 1999).

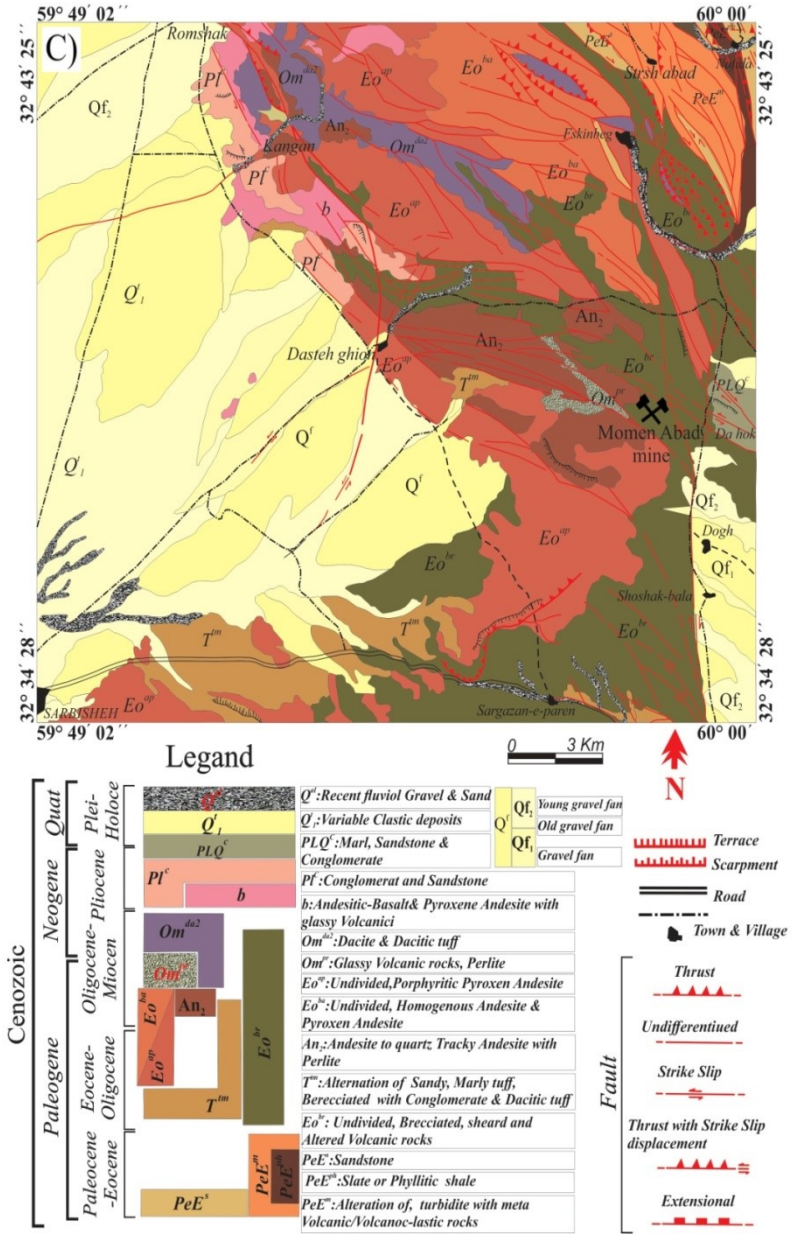

Fig 1. (Continued)

Although the northern and southern limits of magmatism are less fine identified, the accessible geological maps show that the outcrops become even fewer extensive in regions to the south of ~31° N and to the north of ~35° N.

In eastern Iran, the Eocene-Oligocene magmatism created abundant volcanic rocks (lavas and pyroclastic rocks) and subvolcanic rocks. Slight intrusive rocks take place as small isolated plutons. In the Sistan suture zone, the volcanic rocks are integral parts of the regional stratigraphy, which are composed of wide marine sedimentary rocks (flysch) accumulated on an ophiolitic basement from the Late Cretaceous to Eocene. The flysch sequence and related ophiolitic mélange were intruded by the minor plutons noted above. Camp and Griffis (1982) stated the protection of pillow structure in an Eocene porphyritic basalt flow ~100 km west of Zahedan, representative a submarine environment at that time. These authors also showed that the Oligocene volcanism occurred in a subaerial environment.

The volcanic rocks of East-SVC consist of pyroclastic-volcanic rocks. Also, the volcanic units of SVC contain intermediate and low-acidic lavas, while the pyroclastic units contain tuff and ignimbrite. One of the main units of the study area, which extensively outcrops in the east of SVC, contains andesite-dacite with the origin of intermediate calc-alkaline lava with Eocene-Oligocene age. The Eocene-Oligocene (calc-alkaline) magmatic activity is one of the most important magmatic activities in the east of Iran and Sistan Suture Zone (SSZ) (Pang et al. 2012; Mazhari 2016; Tarabi et al. 2019, Yazdi et al. 2019).

The orogenic signature of the eastern SVC volcanic rocks is associated to the mantle source, probably metasomatized by the Sistan subduction in the Late Cretaceous. The trace element features are consistent with the contribution of subducted sediments and fluid released from the subducted slab in magma genesis (Pang et al. 2013).

Based on their mineralogy and texture, the volcanic rocks of East-SVC are divided into three groups including andesite, dacite, and rhyolite. Among these three groups, andesite and dacites rocks have the highest frequency and rhyolite rocks have the lowest frequency, due to altering to bentonite (Tarabi 2018) (Fig 2a). The volcanic dark gray-andesite rocks are extensively outcropped in the East-SVC (Fig 2b), while the volcanic dacite rocks are light gray and outcropped near the volcanic andesite rocks (Fig 2c).

Petrography study of the volcanic rock in East-SVC shows a different micro-texture in plagioclases. These textures are described and classified into 12 types in Table 1. One or more micro-textures usually can be seen in plagioclases of rock groups, which micro-texture domains are separated by resorption surfaces (Renjith 2014). The formation of micro-texture can be related to the relationship between crystal and melt and dynamic behaviors of the crystal during magmatic crystallization (Renjith 2014). In the following, petrography and various micro-textures of plagioclase in andesite, dacite, and rhyolite rocks of East-SVC are described.

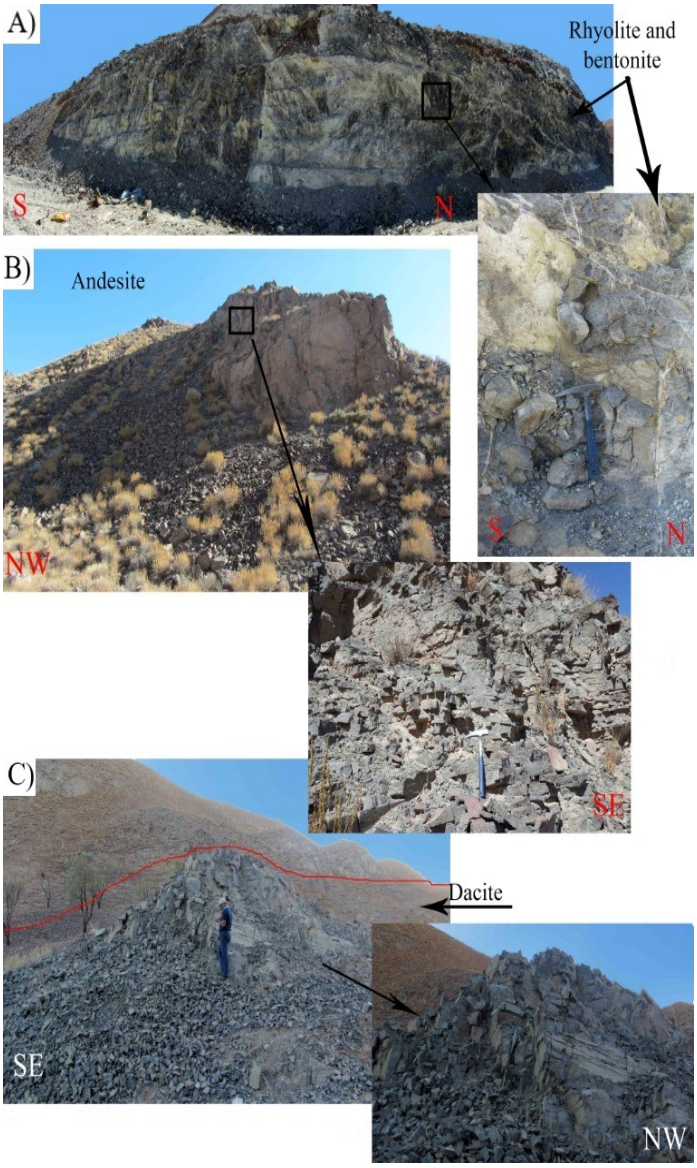

Fig 2. Field outcrops of volcanic rocks of East-SVC. a. Rhyolite rocks, b. Andesite rocks, c. Dacite rocks.

Table 1. The kinds of micro-textures in plagioclases.

	Micro-textures	Abbreviation
1	Coarse-Sieve	CS
2	Fine-Sieve	FS
3	Fine- Scale Oscillatory Zoning	FOZ
4	Rounded Zone Corner	RZC
5	Resorption Surface	RS
6	Micro-Antiperthite (Exsolution)	M-AP
7	Glomerocrysts	GLO
8	Swallow-tail	ST
9	Synneusis	SY
10	Microlites	MIC
11	Broken Crystal	BC
12	Intact Crystal	IC

3. Petrography and micro-textures of the volcanic rock in East-SVC

3.1. Petrography and micro-textures of andesite rocks

Plagioclase phenocrysts (25µm to 1cm) with 65 to 70% frequency are the main felsic minerals of andesite rocks in the study area while the mafic ones include clinopyroxene (augite) and orthopyroxene (enstatite) (Figs 3a-i). The matrix of these rocks contains plagioclase, pyroxene, opaque mineral, and glass (Figs 3d-i). The andesite textures contain glomeroporphyritic, amygdaloidal, trachytic, porphyritic, ophitic, hyalopilitic and microporphyritic (Figs 3a-i).

Clinopyroxene (Augite) is the second main mineral of andesite rocks in the east of SVC, which accounts for about 20-25% of the phenocrysts (Fig 3f-h). This mineral is observed in two forms of phenocryst (25 to 960 µm) and microlite. Orthopyroxenes are often found in form microlite and account for about 5 to 10% of the whole volume of mafic minerals (Fig 3i).

Based on the morphological and microscopic properties of andesite rocks in the east of SVC, different micro-texture of plagioclases can be classified as follows:

- Coarse-Sieve (CS) (Figs 3a, 4a).
- Glomerocrysts morphology (GLO) (Fig 3a).
- Fine-Scale Oscillatory Zoning (FOZ) (Figs 3b, 3d).
- Fine-Sieve (FS) (Fig 3c).
- Microlites (MIC) (Fig 3e).
- Synneusis morphology (SY) (Fig 4b, 4f, 4h).
- Resorption Surface (RS) (Fig 4c, 4d, 4f, 4i).
- Rounded Zone Corner (RZC) (Fig 4c,4d, 4g, 4h).
- Fine-Scale Oscillatory Zoning (FOZ) (Fig 4h)
- FOZ in the Broken Crystal (BC) (Fig 4e).
- Intact Crystal (IC) (Fig 4g).

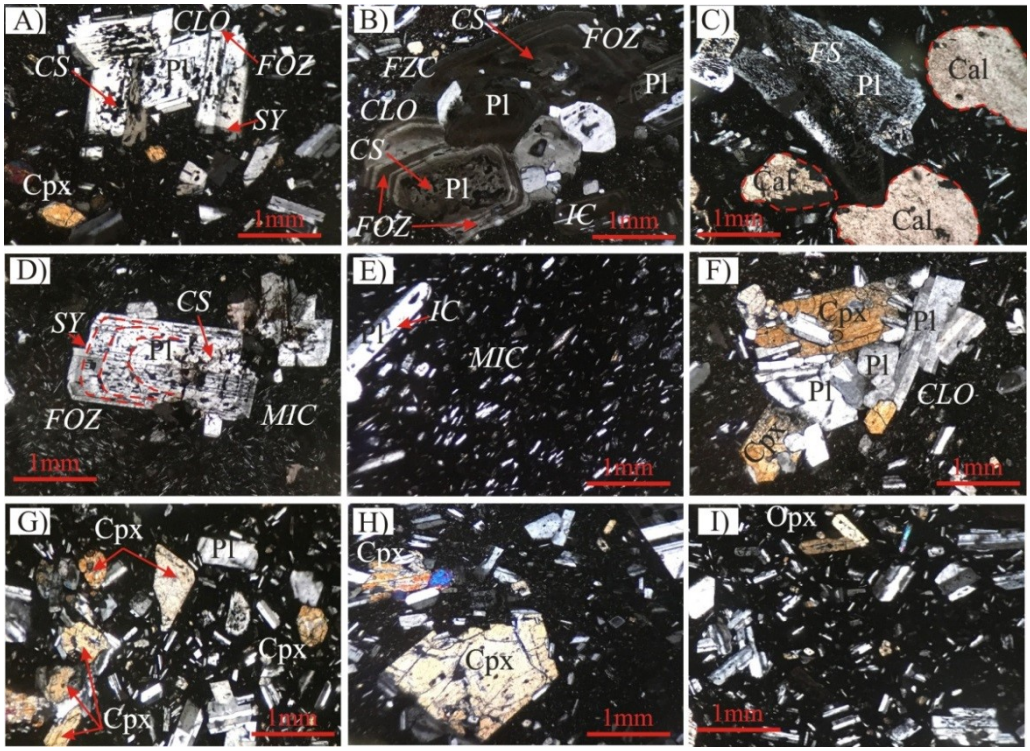

Fig 3. Photomicrograph of andesite rocks (in XPL). a. GLO, CS, SY, and FOZ micro-textures in plagioclases, and microlites of IC plagioclases and clinopyroxene; b. GLO, CS, IC, FZC, and FOZ micro-textures in plagioclases; c. FS micro-textures in plagioclase and amygdaloidal texture; d. FS, FOZ, MIC, and RS micro-textures in plagioclase and porphyritic and trachytic textures; e. IC and MIC micro-textures in plagioclases and trachytic texture; f. Phenocrysts of clinopyroxenes and plagioclases and ophitic texture ; g. Microlites of plagioclases and clinopyroxenes; h. Phenocrysts of clinopyroxene; i. Microlites of plagioclases and orthopyroxenes with hyalopilitic, and microporphyritic textures (Abbreviations from Whitney and Evans (2010)).

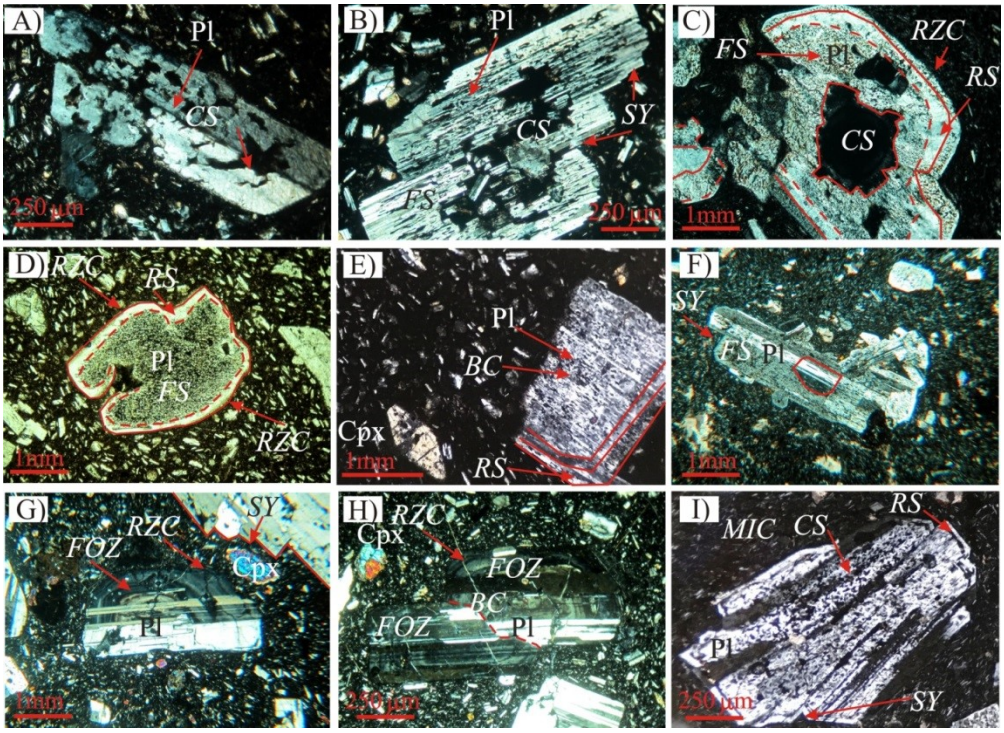

Fig 4. Photomicrograph of andesite rocks (in XPL). a. CS micro-texture in plagioclase; b. CS, in the core and FS in the rim, and SY micro-textures in plagioclase; c. CS, FS, RS, and RZC micro-textures in plagioclase; d. FS, RZC and RS micro-textures in plagioclase; e. BC and FOZ micro-textures in plagioclase; f. FS and SY micro-textures in plagioclase; g. FOZ, RZC and SY micro-textures in plagioclase; h. FOZ, RZC and BC micro-textures in plagioclase; I. CS, CS, SY, and MIC micro-textures in plagioclases.

3.2. Petrography and micro-textures of dacite rocks

The main minerals of dacite are plagioclases, which are found in form of phenocryst and microlite (15µm to over 1cm) and account for 65 to 55% of the whole volume of the main minerals in the rock (Figs 5a-f). Polysynthetic, Carlsbad, and pericline twins, as well as antiperthite exsolution texture, are observed in the studied plagioclase phenocrysts (Figs 5a-c). Sanidine minerals often are seen in the form of microlite with the frequency of 15 to 25%. The acid glassy matrix accounts for 20% of whole minerals in the dacite rock (Fig 5d). Fine-grained crystalline mafic minerals in dacites of East-SVC with less than 15% abundance include orthopyroxene, hornblende, and biotite. The existing orthopyroxene is enstatite, mostly euhedral; the amphiboles include euhedral to subhedral hornbland, and brown euhedral to subhedral biotites (Figs 5d-f). The opacitized rim around the amphiboles and biotites is the most important feature of these minerals (Fig 5f). The predominant texture of East-SVC dacites is trachytic, porphyritic, hyaloporphyritic, vitropheric, and glomeroporphyritic (Figs 5a-d and Figs 6a-f).

Based on the morphological and microscopic properties of dacite rocks in the east of SVC, different micro-texture of plagioclases can be classified as follows:

- Intact crystals (IC) (Fig 5a).
- Fine-Scale Oscillatory Zoning (FOZ) (Figs 5a, 6e).
- Micro-Antiperthite (M-AP) (Fig 5b).
- Coarse-Sieve (CS) (Figs 5b, 6a, 6c, 6e).
- Synneusis morphology (SY) (Fig 5c).
- Swallow-tail morphology (ST) (Figs 6a, 6b).
- Resorption Surface (RS) (Figs 6a, 6b, 6d, 6e).
- Fine-Sieve (FS) (Figs 6d, 6e, 6f).
- Glomerocrysts morphology (GLO) (Fig 6d).

3.3. Petrography and micro-textures of rhyolite rocks

Quartz, plagioclase, and sanidine phenocrysts, in the order of their appearance, are the main minerals of rhyolite in East-SVC (Fig 7a). Biotite is the only mafic mineral of rhyolites (Fig 7b). The textures of rhyolite rocks are hyaloporphyritic with glassy matrix and rarely glomeroporphyritic (Figs 7a-e). Quartz in the form of microlite and phenocryst with the size of 25 to 280 µm accounts for a significant amount of phenocryst, which is found in euhedral, subhedral, anhedral, and angular forms with the cracked surface in a glassy matrix (Fig 7a). Sanidine with both phenocryst and microlite forms and Carlsbad and Lattice twins accounts for 10 % of phenocrysts (25 to 680 µm) (Figs 7a,7e). Besides, phenocryst and microlite of plagioclase with the size of 15 to 980 µm and Polysynthetic, and Carlsbad twins account for approximately 20 to 25 % of phenocrysts (Figs 7d,7f).

Based on the morphological and microscopic properties of rhyolite rocks in the east of SVC, different micro-texture of plagioclases can be classified as follows:

- Coarse-sieve (CS) (Fig 7c).
- Fine-Scale Oscillatory Zoning (FOZ) (Fig 7d).
- Glomerocrysts (GLO) (Fig 7e).
- Fine-Sieve texture (FS) around the rim of crystals (Fig 7e).

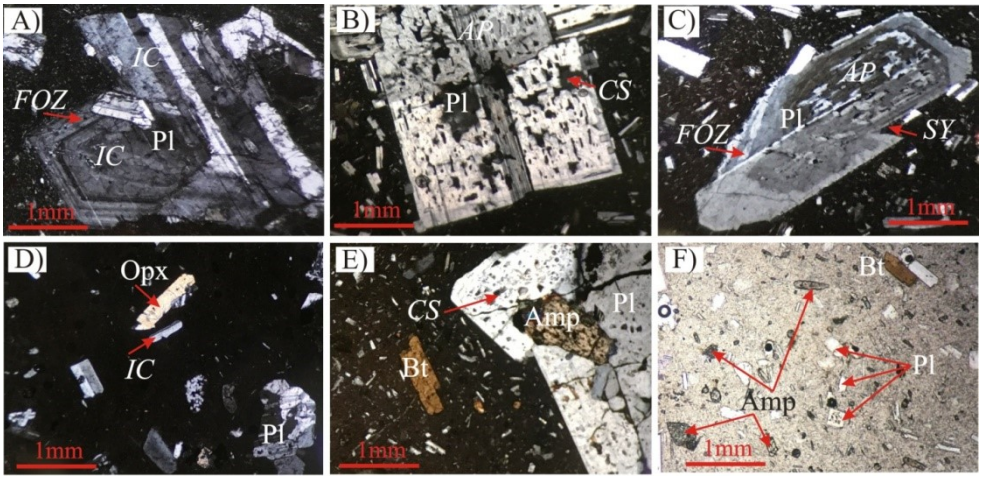

Fig 5. Photomicrograph of dacite rocks (in XPL). a. IC and FOZ micro-texture in plagioclase with Polysynthetic twins; b. CS and M-AP micro-textures in plagioclases; c. M-AP, FOZ, and SY micro-textures in plagioclase; d. IC micro-textures in plagioclase and orthopyroxene and sanidine microlites; e. CS micro-textures in plagioclase with amphibole and biotite; f. Microlites of plagioclases, biotites and amphiboles with opacitized rim (in PPL).

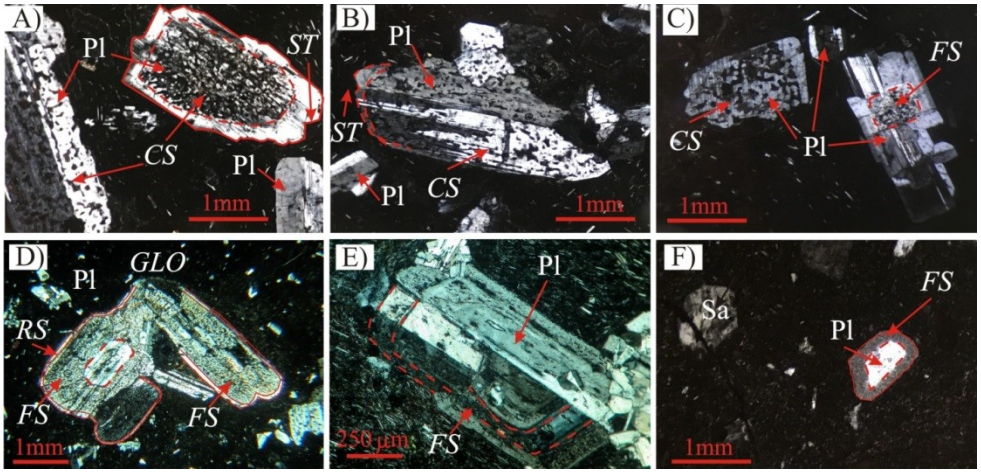

Fig 6. Photomicrograph of dacite rocks (in XPL). a. CS, ST, and CL micro-texture in plagioclase with hyaloporphyritic texture; b. CS and ST micro-textures in plagioclases; c. CS and FS micro-textures in plagioclase with Polysynthetic twins; d. GLO, FS, RS and FS micro-textures in plagioclase; e. FS and FOZ micro-textures in plagioclase with trachytic texture; f. FS micro-textures in rim of plagioclase with vitropheric texture.

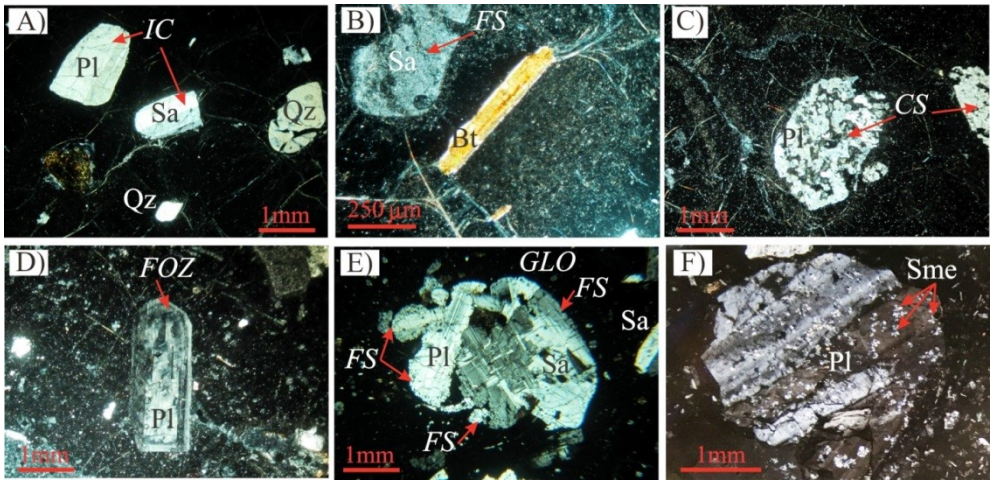

Fig 7. Photomicrograph of rhyolite rocks (in XPL). a. IC micro-textures in plagioclase and sanidine with glassy matrix; b. FS micro-texture in sanidine and showing biotite in rhyolite rocks; c. CS micro-texture in plagioclase with glassy matrix; d. FOZ micro-textures in plagioclase; e. GLO and FS micro-textures in plagioclases; f. Plagioclase with Polysynthetic and Carlsbad twins and alternated to smectite.

4. Material and analytical method

Minerals were selected for analysis using a Cameca SX100 electron microprobe at the *Iran Mineral Processing Research Center*. Quantitative analysis of selected minerals was performed with a 15 keV accelerating voltage using a 20 nA beam current and a 5 μm beam diameter. The counting time at each peak was 20–30 s. Detection limits are in the order of 0.03 wt. % for almost all elements. The result of 103 spot analyses of feldspar, biotite, and pyroxene minerals presented in Supplementary Tables 1, 2, 3 and 4. Standard Name and Standard composition for electron microprobe analysis (EPMA) as follows (Table 2):

Table 2. Standard Name and Standard composition for electron microprobe analysis

Standard Name	*Standard composition for electron microprobe analysis (EPMA)*
F On Fluorite	Fluorite = Ca: 51.3341%, F: 48.6659%
Na On Albite	Albite = Na: 8.7671%, Al: 10.2894%, Si: 32.1311%, O: 48.8124%
Mg On Periclase	Periclase = Mg: 60.3028%, O: 39.6972%
Al On Corundum	Corundum = Al: 52.9242%, O: 47.0758%
Si, Ca On Wollastonite	Wollastonite = Ca: 34.5026%, Si: 24.1772%, O: 41.3203%
K On Orthoclase	Orthoclase = K: 14.0472%, Al: 9.6939%, Si: 30.2715%, O: 45.9874% ,
Ti On Titanite	Titanite = Ti: 100.%
V On Vanadium	Vanadium = V: 100.%
Cr On Chromite	Chromite = Cr: 68.4195%, O: 31.5805%
Mn On Rhodonite	Rhodonite = O: 37.72%, Mg: 0.98%, Si: 21.63%, Ca: 5.2%, Mn: 33.68%, Fe: 0.79%
Fe On Specularite	Specularite = Fe: 69.94%, O: 30.06%
Standard error: 2%	

5. Mineral Chemistry

5.1. Mafic minerals

Pyroxene

There are two kinds of pyroxene in East-SVC andesite rocks including orthopyroxene (enstatite) and clinopyroxene (augite) (Figs 8a-b). The orthopyroxene in East-SVC dacite rocks has enstatite composition (Figs 8a-b) (Supplementary Table 1).

Biotite

Biotites of East-SVC dacites are mg-biotites (Figs. 9a-b) (Supplementary Table 2).

Opaque minerals

Ilmenite is the dominant opaque mineral in the East-SVC volcanic rocks.

5.2. Felsic mineral

Feldspar

The plagioclase chemical compositions of East-SVC andesite are labradorite and bytownite (Figs 10a,11a,13a,17a) while the dacite ones are andesine and labradorite (Figs 12a,14a). The chemical analysis of antiperthite exsolution micro-textures existing in dacite samples showed that matrix of plagioclases with andesine composition and antiperthite spots is orthoclase (Figs 15a,16a). The process of chemical variations in different micro-textures (IC, CS, FG, and GLO) of andesite and dacite plagioclases is explained in the section of interpretation of plagioclase profile (Tables supplement 3, 4).

6. Discussion

6.1. Interpretation of plagioclases micro-textures of compositions in the East-SVC volcanic rocks

The chemistry of plagioclases with different micro-textures was evaluated in two andesite and dacite rock groups in East-SVC:

6.1.1. The chemical composition of plagioclases with CS micro-texture

CS texture is often seen in plagioclase crystals (Figs 3a-d; 4a-c; Figs 5b; Figs 6a-c). The crystals chemistry of East-SVC andesite with CS texture is labradorite to bytownite and the changes trend of anorthite composition from rim-to-rim of plagioclase crystal shows an increase in anorthite from core-to-rim of the crystal; however, the changes are not significant and are limited to labradorite to bytownite (Figs 10a and 11a).

The plagioclase chemical composition of East-SVC dacite with CS texture is andesine to labradorite. In plagioclase, the change trend of anorthite is normal from rim-to-rim; i.e., from core-to-rim, the anorthite content is reduced while albite is increased (Figs 12a). The CS texture along with oscillatory zoning is observed in the rim of plagioclase crystals (Fig 12d). In this type of crystal, the most external part of the crystal is rich with anorthite, and the changes trend of anorthite in the crystalline rim of the zoning section has a significant change and is labradorite. The chemical changes trends of the sieve texture show a variation in basic magma in dacitic magma. The occurrence of this condition leads to an increase in temperature, partial melting of the central part of the crystal, and formation of CS texture, and, consequently, the chemical changes of magma in the chamber causes the formation of An-enrichment in the outer layer of the plagioclase crystal (Fig 12d).

6.1.2. The chemical composition of plagioclases with FS micro-texture

The FS micro-textures with different morphology in the rim, core, and even total crystal or along with other micro-texture are seen in East-SVC volcanic rocks.

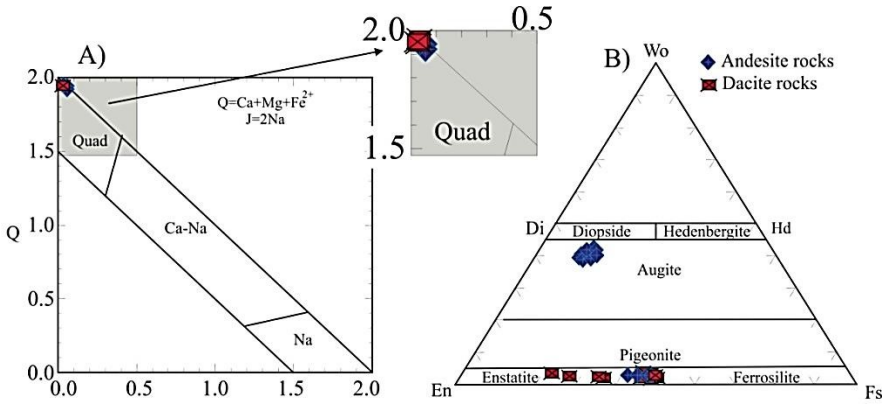

Fig 8. a. Q-J diagram for the pyroxenes, the pyroxenes in the Quad area are classified on the pyroxene quadrilateral Wo-En-Fs diagram with normalized Ca, Mg, and ΣFe (:Fe^{2+}+ Fe^{3+}+ Mn) atoms; b. Plot of pyroxenes composition of andesite and dacite rocks East-SVC in Wollastonite (Wo)-Enstatite (En)-Ferrosilite (Fs) diagram (Morimoto 1989).

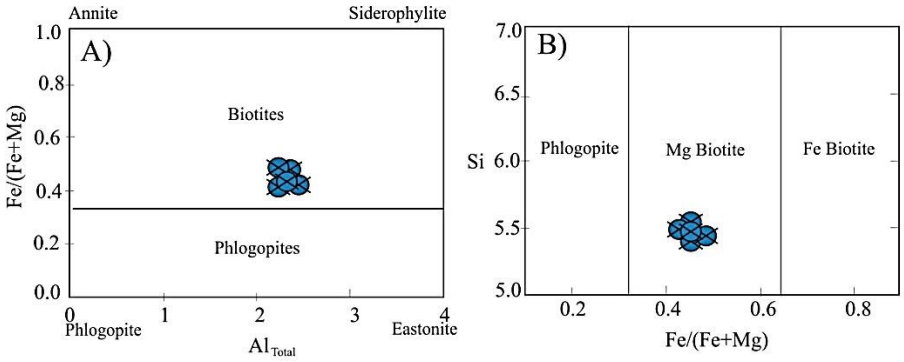

Fig 9. a. Fe/(Fe+Mg)-Al_{total} diagram showing the composition of biotite, b) Si-Fe/(Fe+Mg) diagram showing the biotite in the dacite rocks are Mg-biotite.

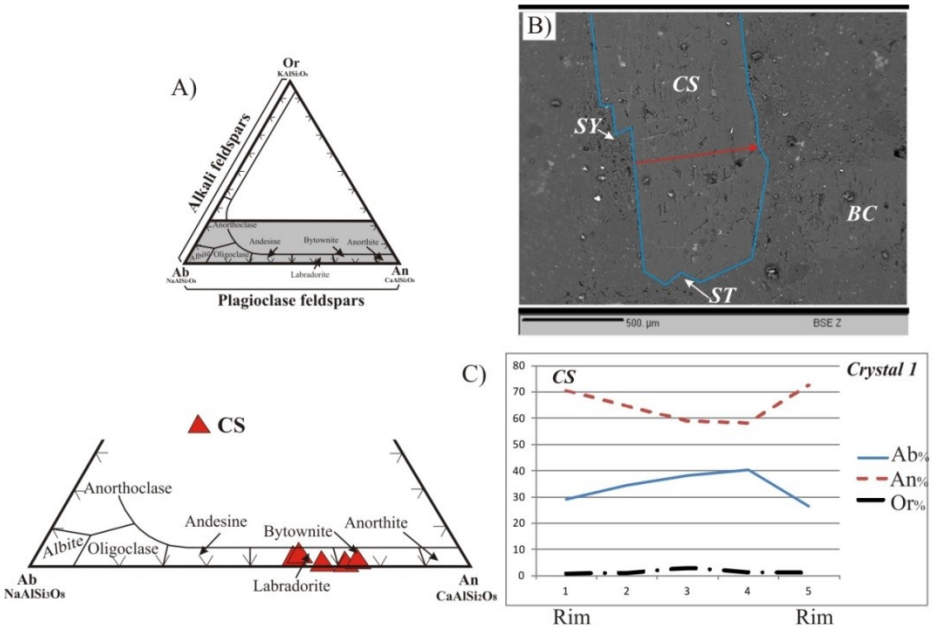

Fig 10. Plagioclase with CS micro-textures in andesitic rocks. a. Chemical composition of plagioclase; b. BSE image; c. Rim-to-rim profiles of An, Ab, Or %.

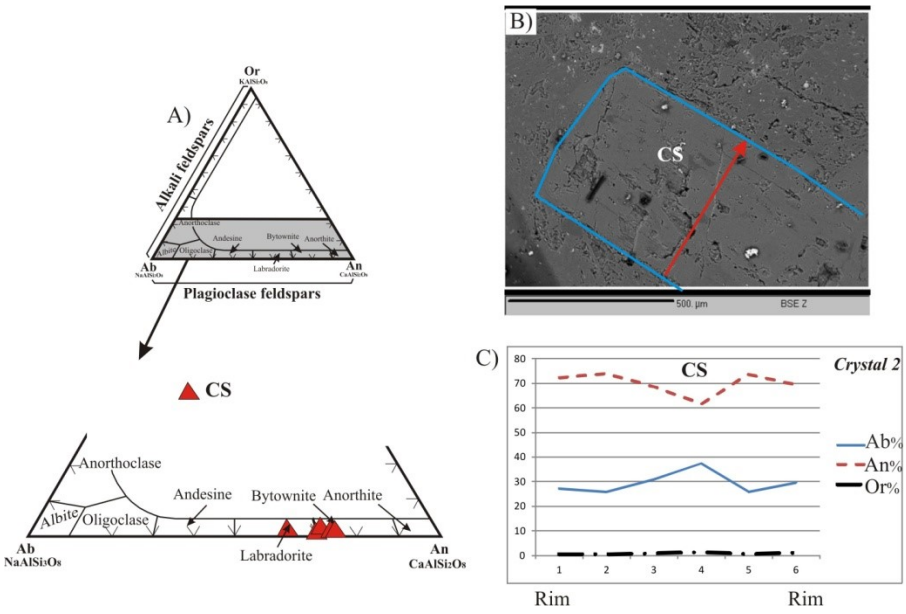

Fig 11. Plagioclase with CS micro-textures in andesitic rocks. a,b,c. Corresponding rim-to-rim compositional profiles of An, Ab, Or %.

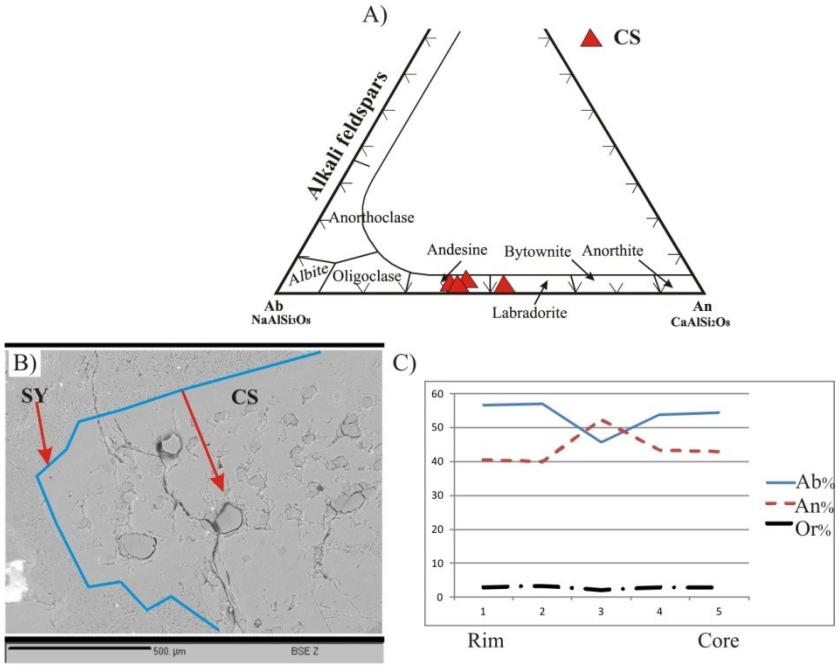

Fig 12. Plagioclase with CS micro-textures in dacite rocks. a. Chemical composition of plagioclase; b. BSE image; c. Rim-to-core profiles of An, Ab, Or %.

In East-SVC andesite rocks, the chemical composition of FS micro-texture is bytownite and labradorite and the rim-to-rim change trend of anorthite shows an oscillatory zoning (Figs 13a-c). This variation in the chemistry of plagioclase demonstrates the changes in chemical composition of magma during crystallization, which caused the formation of FS micro-texture. Also, the Synneusis texture is observed in the rim of the crystals, which is the result of the dynamic motion of the crystal during its growth in the magma chamber.

In the dacite rock group, FS micro-texture is often observed along with other micro-textures. In antiperhite crystals, this texture is formed as alkali-feldspar crystals with a lower melting point (Figs 14a-c). FS micro-texture is formed by raising the temperature of magma and partial melting.

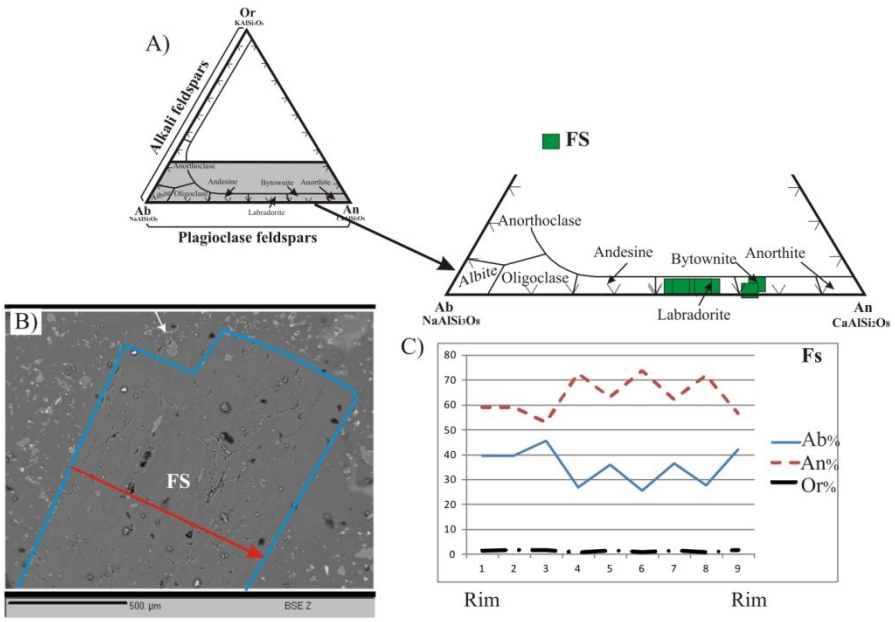

Fig 13. Plagioclase with Fs micro-textures in andesitic rocks. a. Chemical composition of plagioclase; b. BSE image; c. Rim-to-core profiles of An, Ab, Or %.

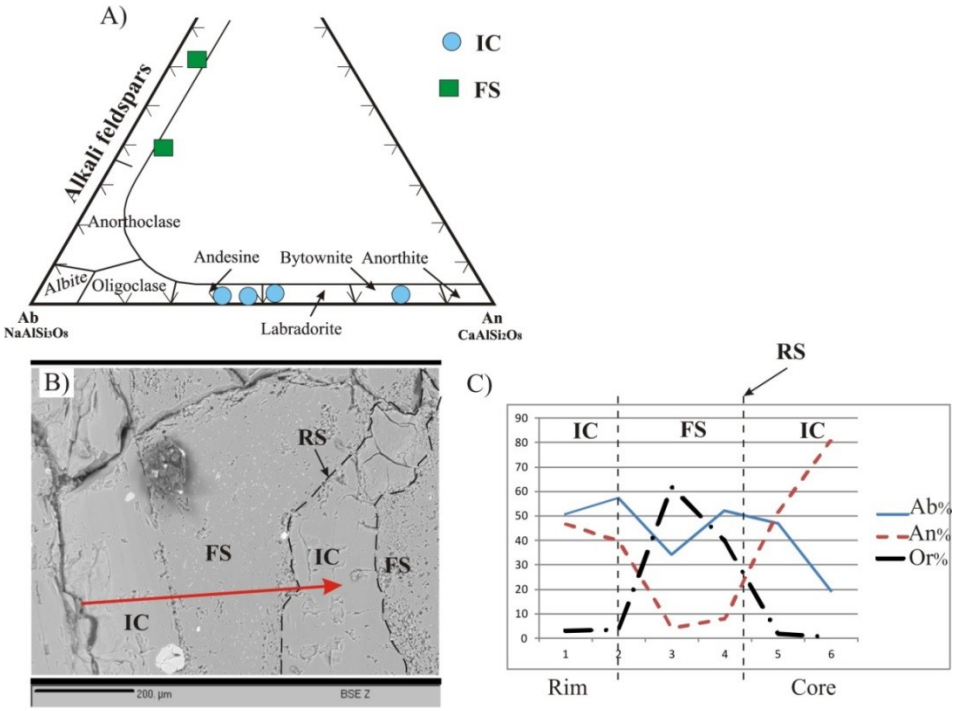

Fig 14. Plagioclase with FS micro-textures in dacite rocks. a. Chemical composition of plagioclase; b. BSE image; c. Rim-to-rim profiles of An, Ab, Or %.

6.1.3. The chemical composition of plagioclases with exsolution micro-texture

The exsolution micro-textures are only observed in dacite rocks East-SVC. Besides, since the changes in temperature or the chemical composition of the magma lead to melting of some part of the crystal with a lower melting point, these micro-textures are along with FS texture. The chemistry of plagioclase with exsolution micro-texture is andesine to bytownite and the composition of alkali-feldspar is orthoclase (Figs 15a-c) and (Figs 16a-c).

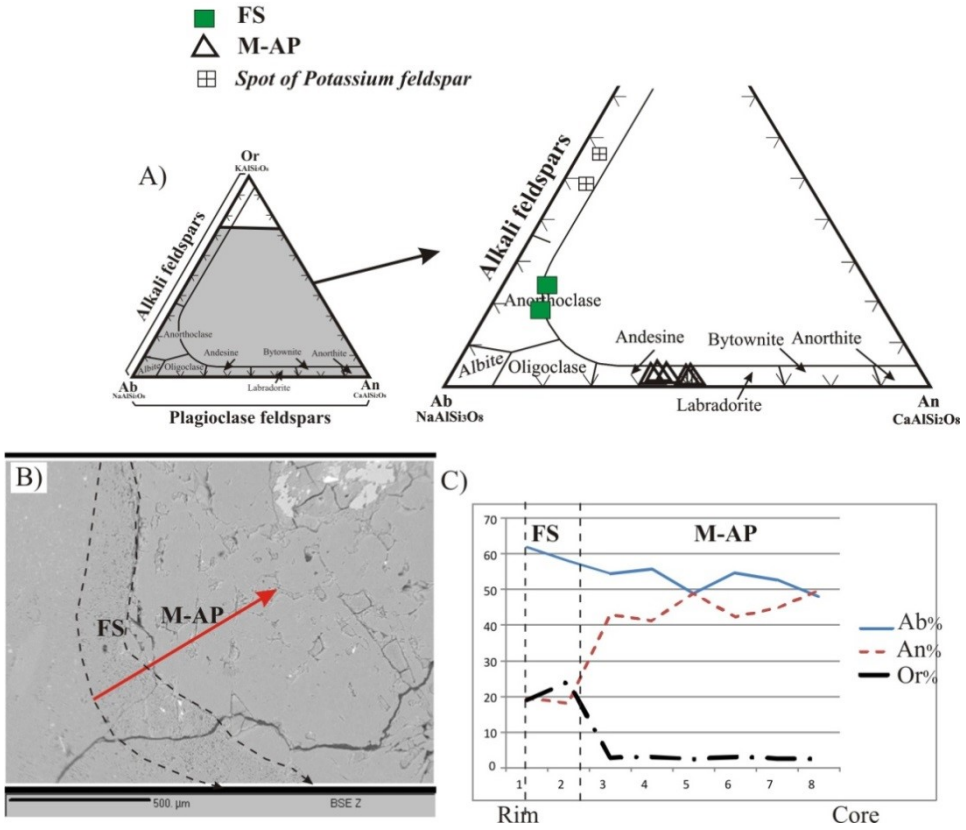

Fig 15. Plagioclase with M-AP micro-textures in dacite rocks. a. Chemical composition of plagioclase; b. BSE image; c. Rim-to-core profiles of An, Ab, and Or %.

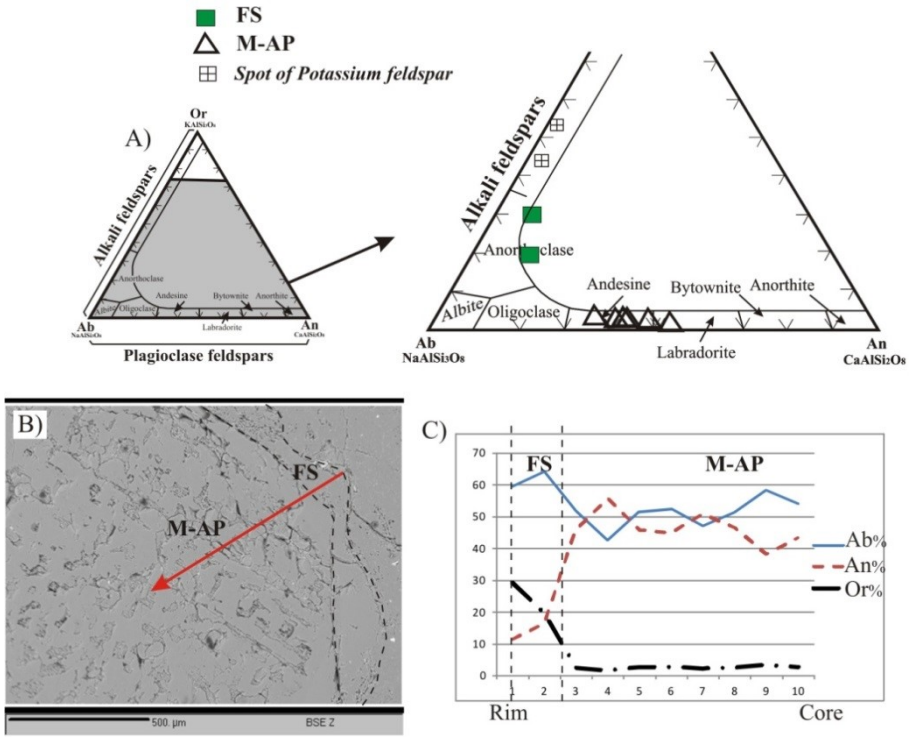

Fig 16. Plagioclase with M-AP micro-textures in dacite rocks. a. Chemical composition of plagioclase; b. BSE image; c. Rim-to-core profiles of An, Ab, and Or %.

6.1.4. The chemical composition of plagioclases with GLO micro-texture

Based on the chemical analysis of three crystals of plagioclase in the andesite rocks East-SVC with GLO morphology, they fall in the range of bytownite to labradorite. Enrichment of anorthite (core) and Ab (rim) in crystals 1 and 2 represents the normal crystallization process (Figs 17a-c). However, in crystal 3, the crystallization process is abnormal, because the rim of crystal shows An-enrichment. It has to be noted that the changes trend of anorthite occurs in an oscillatory form (Fig 17d). Further, the crystal 3 was crystallized after the recharge of basic magma and change of chemical composition of the magma.

6.1.5. The chemical composition of plagioclase with IC

The intact crystals do not have any sieve textures; however, in the rim of some intact crystals, Synneusis textures are observed. This texture was formed in the magma chamber before crystallization due to the motion of intact crystal. In the andesite rocks East-SVC, the chemical composition of intact crystals, which is bytownite, is more basic than other crystals (Figs 18 a-c). It must be added that some crystals have an oscillatory zoning. Intact crystals of the dacite rock group have a higher percentage of anorthite compared to other crystals and are labradorite (Figs 18 d-f). Since in volcanic rocks, intact crystals are formed in the magma chamber after temperature and chemical changes, these crystals are more basic than other micro-textures.

6.1.6. The chemical composition of feldspar with MIC

Several microlite crystals of dacite and andesite rock groups were analyzed. Their chemical composition was andesine, orthoclase, and bytownite. Presence of various percentages of anorthite in microlite can be due to the recharge of basic magma at the base of the magma chamber on the magmatic system; however, this factor did not change the complete chemical composition of the magma of East-SVC rocks. Therefore, during the final crystallization of magma (microlite) in andesite and dacite groups, crystals with a low amount of anorthite were formed (Supplementary Table 3, 4).

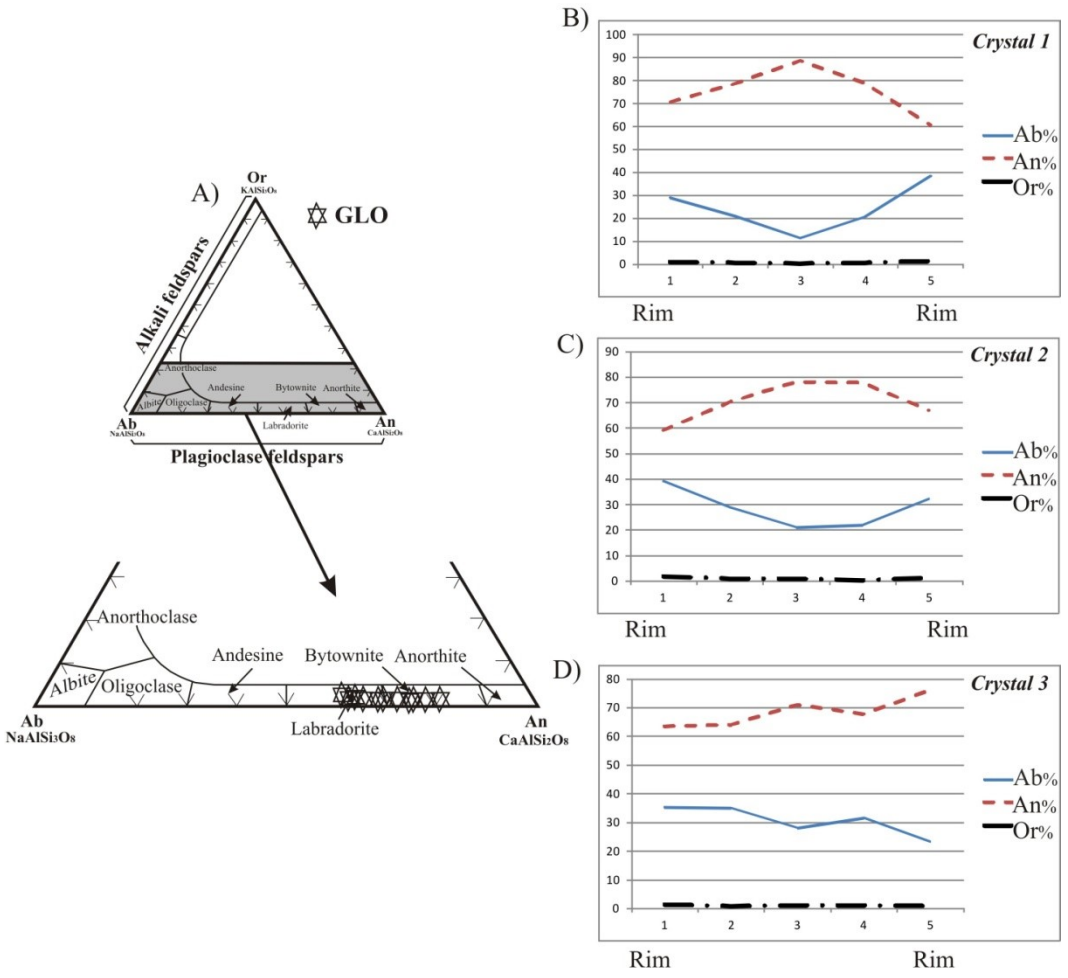

Fig 17. Plagioclase with GLO micro-textures in andesitic rocks. a. Chemical composition of plagioclase; b, c, d. Rim-to-rim profiles of An, Ab, and Or % from crystal 1, 2 and 3.

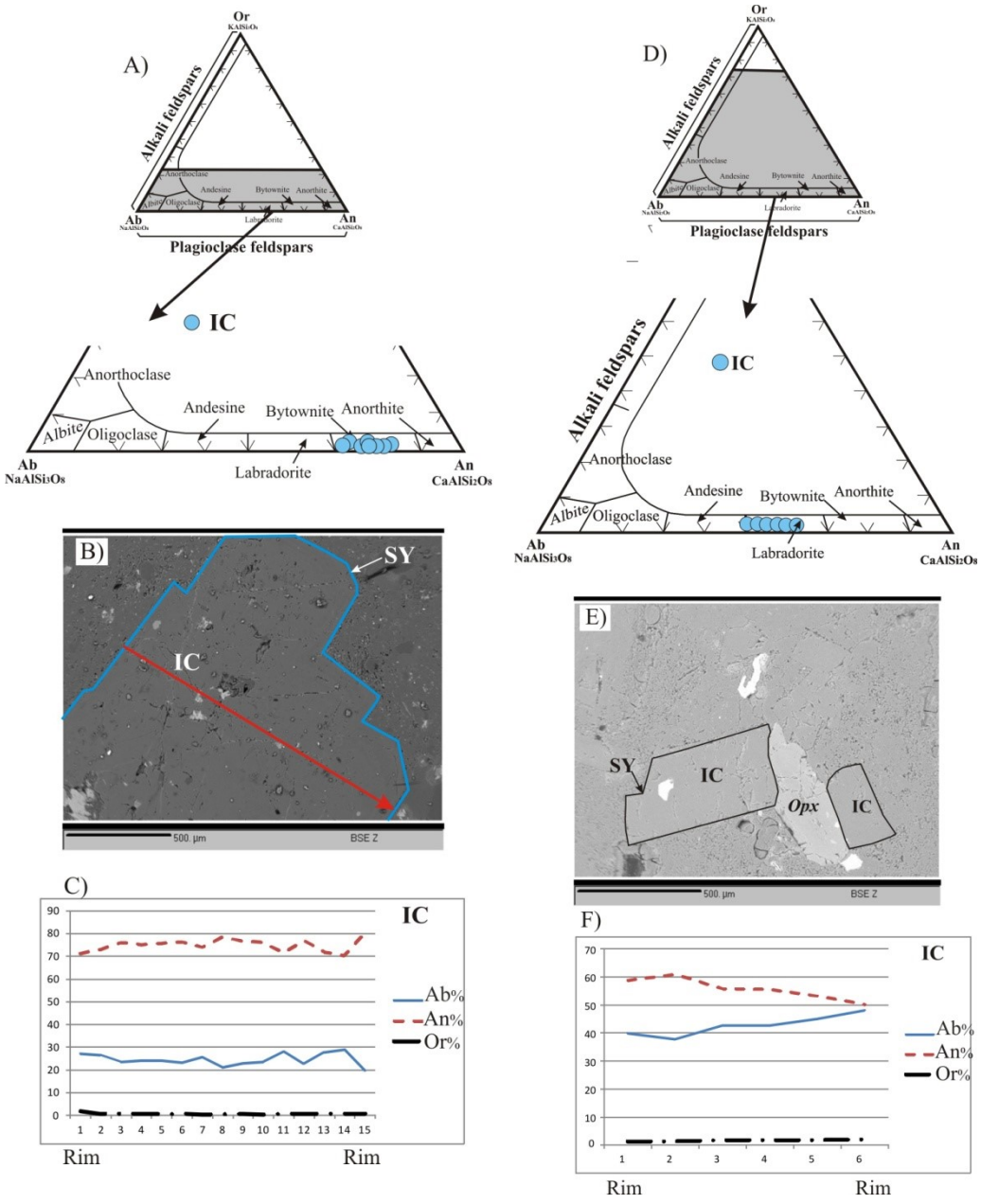

Fig 18. a. Chemical composition of Plagioclase with IC micro-textures in andesitic rocks; b. BSE image of Plagioclase with IC micro-textures in andesitic rocks; c. Rim-to-rim profiles of An, Ab, and Or % in andesitic rocks; d. Chemical composition of Plagioclase with IC micro-textures in dacite rocks; e. BSE image of Plagioclase with IC micro-textures in dacite rocks; f. Rim-to-rim profiles of An, Ab, and Or % in dacite rocks.

6.2. Determination of crystallization condition by using pyroxene chemistry

The evaluation of chemical changes trend of clinopyroxene crystal in andesite rocks East-SVC indicated very limited changes in abundance of elements. Accordingly, the depletion of Fe, Si, Al, and Ti and enrichment in Mg and Ca are observed from core-to-rim (Supplementary Table 1). Such little changes in oscillatory zoning of pyroxene can be interpreted by recharge event and magmatic convective motion in the magmatic chamber. According to Deer et al. (1966), the Mg-rich zones were crystallized in primary mantel magma at high temperature, while the Fe-rich rims were formed in the next step by more differentiated magma. Observing a low difference in Fe and Mg between core and rim of clinopyroxene suggests their crystallization in the same magma chamber and their very little changes due to magmatic recharge with the same origin.

Comparing the changes in the amounts of Ca, Na, Al, Mg, and Mn with the increase in $Mg^{\#}$ in pyroxenes reveals that the changes in Na, Al, and Mn are not significant. However, the changes in Mg and Ca present a very low increase while Fe^{2+} variations show a

decreasing trend (Supplementary Table 1).It has been evidenced that the increasing trend of Ca can occur due to magmatic differentiation because magmatic differentiation results in an increase in the alkaline elements, leading to a consequent increase in Mg due to the recharge of basic magma at the base of the magma chamber.

6.2.1. Thermobarometry

Pyroxene is a mineral reflecting the physical conditions (i.e., temperature and pressure) of magma during the crystallization. In igneous rocks petrology, thermobarometric equations are used to evaluate the temperature and pressure of crystallization of minerals. Therefore, to determine the temperature and pressure, various methods of clinopyroxene chemistry of SVC andesite rocks are applied.

In the method proposed in (Soesoo 1997), the temperature and pressure of the magma are defined by two indices: X_{PT} and Y_{PT}. In this method, the temperature and pressure are plotted and the axes X and Y are defined based on X_{PT} and Y_{PT} indexes (Figs 19a-b). Eq. 1 is applied to calculate X_{PT} and Y_{PT} in order to determine the points analyzed points in the diagram (Figs 19a-b).

In clinopyroxene of the andesite rocks East-SVC, the pressure and temperature were calculated to be less than 2 to 5 kbar and 1150°C using calculated values of X_{PT} and Y_{PT} by Eq. 1 (Figs 19a-b).

In thermometer method of Lindsley (1983), the crystallization temperature of clinopyroxene and orthopyroxene was calculated to be 1100 to 700 °C and 700 to 1100 °C, respectively, based on a molecular percentage of wollastonite-enstatite-ferrosilite (Fig 20).

The clinopyroxenes of andesite rocks East-SVC are plotting in low-pressure clinopyroxene (Figs 19c-d) based on the Cr_2O_3 vs. Mg and Al_2O_3 vs. TiO_2 in clinopyroxene (Elthon 1987) diagrams.

The results of various methods for determining temperate and pressure of crystallization in clinopyroxene of andesite rocks East-SVC showed an irregular increasing and decreasing pattern of temperature and pressure from core-to-rim (Supplementary Table 1). Moreover, the oscillatory zoning with little change in the chemical composition of clinopyroxene during the magma crystallization occurred due to temperature changes by recharge event. The pressure changes during the crystallization of clinopyroxene also occurred due to movement from the depth of the magma chamber to the surface of the earth and an increasing magma vapor pressure.

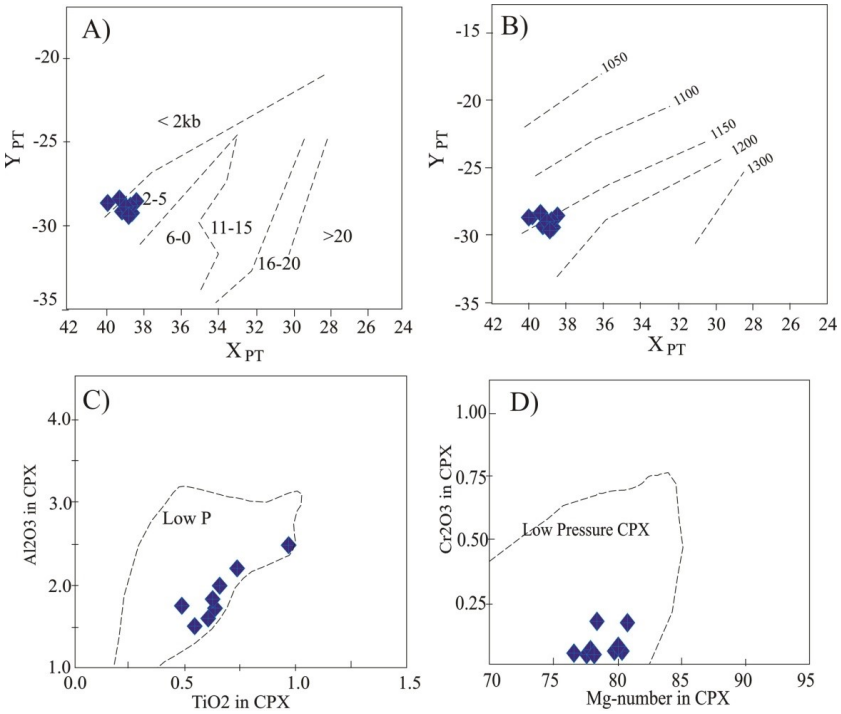

Fig 19. a. and b. X_{PT}-Y_{PT} diagram of clinopyroxene showing crystallization PT-conditions of andesite rocks East-SVC; c. The TiO_2-Al_2O_3 contents of clinopyroxenes from andesite rocks East-SVC, Samples plot in low-pressure field; d. Cr_2O_3- Mg in clinopyroxene diagram showing the samples plot in low-pressure field. Eq. 1: (X_{PT}= $0.446\times SiO_2+0.187\times TiO_2-0.404\times Al_2O_3+0.346\times FeO^{(tot)}-0.052\times MnO+0.309\times MgO+0.431$ CaO-0.446 Na_2O, and Y_{PT}= $-0.369\times SiO_2+0.535\times TiO_2-0.317\times Al_2O_3+0.323\times FeO^{(tot)}+0.235\times MnO-0.516\times MgO$ $0.167\times CaO-0.153\times Na_2O$).

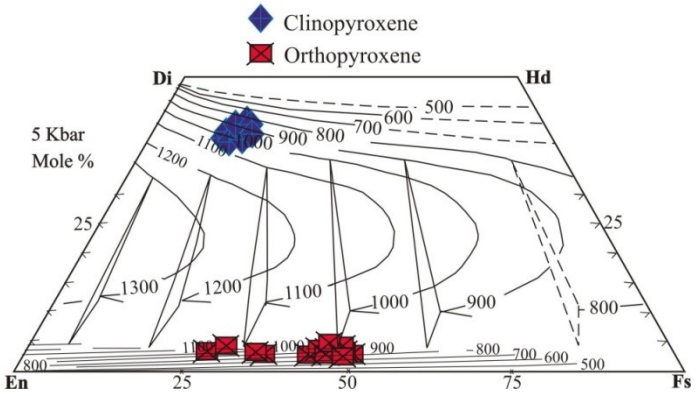

Fig 20. Projection of recalculated pyroxene end-member compositions in Di-Hd-En-Fs thermometry diagram (Lindsley 1983). Clinopyroxenes from andesite rocks and orthopyroxenes from andesite and dacite rocks.

6.2.2. Magmatic series and tectonic setting

The chemistry of clinopyroxene depends on the chemistry of magma and setting where the lava is formed; therefore, this mineral is used to determine the tectonic setting of the rock formation. The presence of Al, Ti, Ca, Si, and Na in clinopyroxene depends on the alkalinity degree of parental magma (Le Base 1962 and Leterrier et al. 1982). The chemical chemistry of clinopyroxene is rich in Ca and in Ti vs. Ca+Na and Ti vs. Al_{total} diagrams (Leterrier et al. 1982) shows a calc-alkaline affinity (Figs 21a-b). Here, SiO_2 vs. Al_2O_3 (Le Base 1962) was used to determine the tectonic setting of clinopyroxene formation (Fig 22a). According to Fig. 22b, the chemical composition of clinopyroxene is in VAB while based on F1 and F2 diagram (Nisbet and Pearce 1977), the tectonic setting of clinopyroxene formation is VAB and OBI.

Based on the chemical composition of clinopyroxenes with a low Ti (0.005-0.028) and enrichment in Ca (0.787-0.861) and Si (1.863-1.934), as well as its calc-alkaline affinity, the tectonic setting of the andesite rocks East-SVC is VAB (Beccaluva et al. 1989).

6.3. Determining crystallization conditions by using biotite chemistry

In the ASPE diagram, the chemical composition of mica in East-SVC dacite rocks is in biotite area (Spear 1984; Deer et al. 1966) and the variations of Fe and Al are very little in ASPE diagram. Thus, the variations of these elements have no increasing or decreasing trend and show a cumulate pattern, which a characteristics feature of biotites without crustal contamination (Shabani et al. 2010) (Fig 9a).

Biotites microprobe results show that these minerals have a high content of MgO (12.17-12.76) and a low content of Al_2O_3 (13.22-13.86). As shown in Supplementary Table 2, the $Mg/(Mg+Fe^{2+})$ ratio these minerals varies between 0.55 and 0.59. Besides, the studied biotites have almost a low FeO content (15.90-17.86). Therefore, the chemical properties of biotites show that these minerals are primary and have been directly crystallized in magma (Stone 2000). Moreover, in Foster (1960) diagram, biotites are the Mg-biotite type (Fig 9b).

6.3.1. Thermobarometry

According to the results of biotite chemistry analysis (Supplementary Table 2), Si was substituted with Al^{IV}, indicating that the crystallization of biotite occurred at high temperatures (Deer et al. 1966). In addition, according to the Nachit et al. (1985) diagram, biotites were crystallized at 750 °C.

Uchida (2007) proposed a positive linear relationship between the amount of Al^T biotite and magma crystallization pressure:

Eq. 2 $$P_{(Kb)} = 3.03 \times Al^T - 6.53(\pm 0.33)$$

Based on biotite barometry using Eq. 2, the mean crystallization pressure of volcanic rocks in East-SVC andesite is about 0.578 kbar. Also, considering the equation error, the crystallization pressure is about 0.611-0.545 kbar (Table 3).

6.3.2. The magmatic series

Since the chemical chemistry of biotite indicates the properties of parental magma (Spear 1984), it is used to determine the nature of parental magma. Accordingly, the chemical composition of biotites in East-SVC dacite rocks shows calc-alkaline magma nature in diagrams (Figs 23a-d) proposed by Abdel-Rahman (1994). Furthermore, in Al^{total}-Mg diagram (Henry et al. 2005), biotites shows a calc-alkaline affinity (Fig 24), which is in agreement with those of Abdel-Rahman (1994) diagrams.

Table 3. determination of pressure based on the amount of Al in biotites of East-SVC dacite (pressure in Kbar).

Point.No	Al^T	P(Kbar)
30	2.342	0.57
31	2.370	0.65
32	2.384	0.69
33	2.291	0.41
34	2.316	0.49
35	2.373	0.66
Average	2.346	0.578

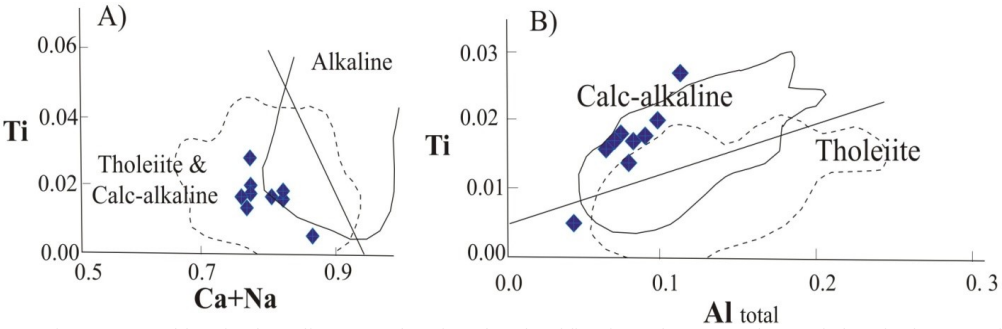

Fig 21. A. Ti-Ca+Na and b. Ti-Al_{total} diagrams showing the classification of magmas base of chemical composition of clinopyroxene, samples plot in calc-alkaline field.

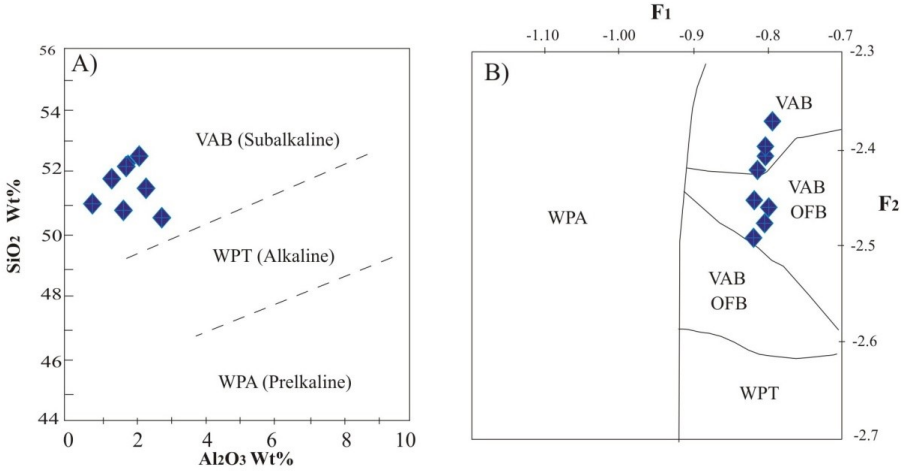

Fig 22. a. SiO_2-Al_2O_3 contents of clinopyroxene diagram and b. F1-F2 of clinopyroxene diagram are showing the tectonic setting of andesite rocks.

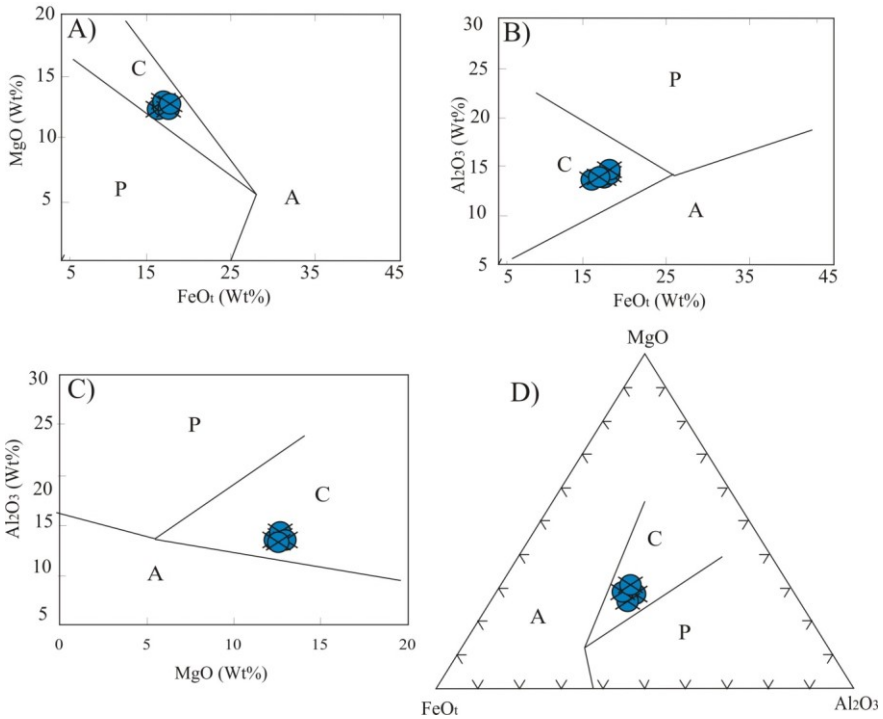

Fig 23. Discrimination diagrams showing the classification of magmas after Abdel-Rahman (1994) samples plot in field C (calc-alkaline). a. MgO- FeO_t wt% contents of biotite, b. Al_2O_3-FeO_t wt% contents of biotite, c. Al_2O_3-MgO wt% contents of biotite, d. Al_2O_3-MgO- FeO_t wt% of biotite.

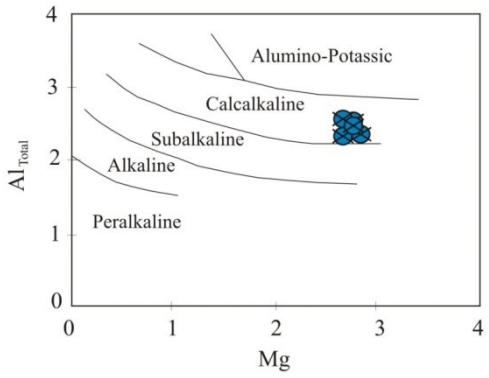

Fig 24. Discrimination Al_{total}-Mg diagram showing the classification of magmas after Henry et al. 2005 samples plot in calc-alkaline field.

6.3.3. Magma chamber process and plumbing model

Various micro-textures were identified in andesite, dacite, and rhyolite rock groups of East-SVC. These micro-textures, which are not specific to a particular rock group of volcanic rocks of the eastern SVC, are caused by different factors that can be classified into two different groups: (1) Growth micro-textures in the form of CS, FS, FOZ, and RS formed when the equilibrium at the crystal-melt interface was fluctuated due to alteration in temperature or H_2O or pressure or composition of the magma; and (2) Morphological micro-textures, such as GLO, SY, ST, MIC, and BC that are the products of dynamic magma processes including convection, degassing, and an explosive eruption. Each texture has been developed under a particular magmatic environment.

Construing their stratigraphy, valuable information can be provided regarding the sequence of magma process included from deep source to areal eruption. Some clue about the order of crystallization can be revealed by phenocryst size (e.g., Marsh 1998; Yu et al. 2012). Among the three identified phenocryst size-groups, small (<1 mm) and large (3-5 mm) groups represent younger and older plagioclase populations, respectively. Microlites are the late stage crystallization products of undercooling-associated syn-eruption or just pre-eruption. Similarly, BC and ST micro-textures are also created at the ultimate stage of eruption-related magma process. However, the cores of large phenocrysts present the older plagioclase population in the studied rocks because their An-rich cores show CS morphology only at the cores of large phenocrysts and are devoid of small and medium-size phenocrysts, the latter born after the CS developments process. After developing the CS texture, the majority of the grains have further re-grown and developed multiple textural domains such as FS and FOZ toward the rim (Figs 3a-d; 4b,c,I; 6a,b,d-f; 12d). However, after the development of the CS domain, a few grains just have been welded together as GLO. Subsequently, by developing a common outer shell with FS or FOZ texture, they re-grow as a single grain (Figs 3a-b; 6d). Hence, the glomerocryst formation postdates the CS and predates FS, and FOZ textural formations. Most of the phenocrysts with CS micro-texture in their core are surrounded by FS and FOZ micro-texture, suggesting that the occurrence of CS formation postdates the formation of both. Since no correlation is found in the incidence of FS and FOZ micro-textures between the phenocrysts, predicting their genetic is difficult. Plagioclase laths within the FOZ domain suggest that SY and FOZ have been developed instantaneously.

Therefore, it can be comprehended that after developing the CS morphology, micro-textures like FS, FOZ, GLO, and SY are developed from a complex and repeated magma process occurring in the shallow chamber before the eruption.

In plagioclase crystals with sieve (CS and FS) micro-textures, the change trend of FeO is not as same as anorthite. Therefore, in these crystals, the changes of chemical composition of magma cannot be a function of sieve micro-textures; rather, other factors such as temperature rise or H_2O fugacity changes in the magma can take a role in the formation of these micro-textures. Moreover, temperature variation can occur due to self-mixing in the magma chamber.

That self-mixing environment was enhanced by the recharge of hotter magma at the base of the magma chamber (e.g., Huppert et al. 1982; Couch et al. 2001) (Fig 25). The magma chamber during the self-mixing process might have experienced undercooling by degassing or water exsolution followed by violent aerial eruption creating microlites broken and swallow-tail crystals (Fig 25).

The majority of IC has a higher anorthite percentage compared to plagioclases with various micro-textures. In addition, the variation trend of Fe, Mg, Ti, and Ca elements in clinopyroxene of andesite rocks East-SVC is very limited and oscillatory. Frequent recharge in the magma chamber can be a cause for an oscillating state with minor changes in clinopyroxene.

According to the chemistry of clinopyroxene and biotite in East-SVC andesite and dacite rocks, the magmatic series was calc-alkaline and their tectonic setting was related to VAB. Besides, the results of clinopyroxene a biotite chemistry analysis were in agreement with those reported by Pang et al. (2013).

The thermobarometry evaluation using pyroxene and biotite chemistry showed that the temperature ranges for andesite rocks East-SVC were between 700 and 1150 °C and the pressure was less than 2 kbar. The reason for these changes can be related to the size of the magmatic chamber.

Considering the performed studies, the formation of different micro-textures in plagioclases of East-SVC volcanic rocks is not related to the changes of chemical composition of magma; rather, it can be due to the related to the variations of temperature, H_2O fugacity, and recharge event in the magma chamber.

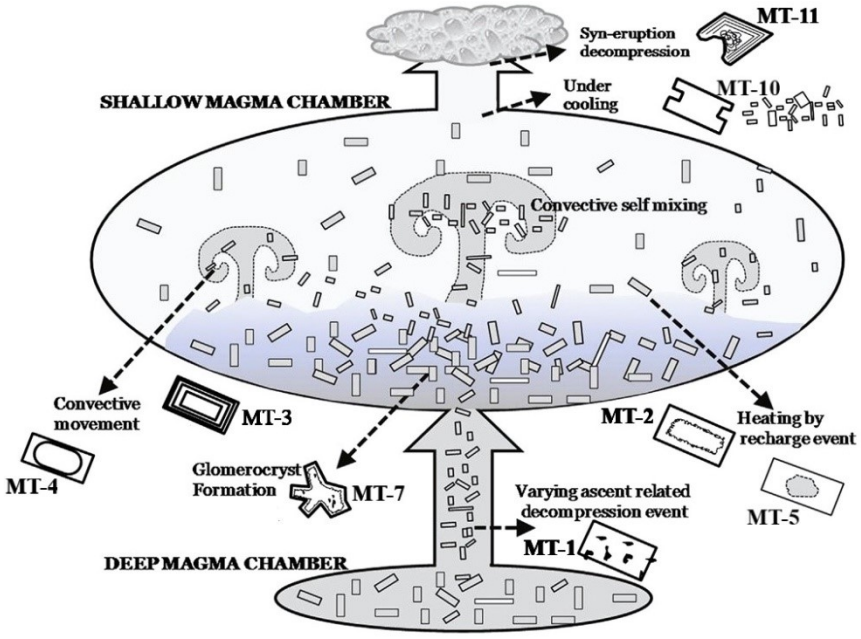

Fig 25. Schematic model of crystallization dynamics and magma plumbing system (modified after Renjith 2014).

Moreover, the occurrence of these changes can be associated with the self-mixing process in the magma chamber. Renjith (2014) presented the schematic image of the self-mixing process and its mechanism as a triggering factor for the physical and chemical changes in the magma chamber, which results in the formation of various micro-textures in plagioclases of volcanic rocks in Barren Island. Using this model, we can describe the formation mechanism of various micro-textures in East-SVC volcanic rocks.

At the early stage, water-saturated high-temperature magma has undergone extensive crystallization at the deeper chamber in a stable magmatic environment producing An-rich plagioclase (Fig 25). As shown in Fig 25, when this crystal-rich magma ascended to the shallow chamber, these crystals have undergone a varying rate of dissolution leading to the development of CS morphologies with varying size, shape, and density (number of CS per unit area). Variation in the intensity of dissolution may be caused by the difference in the rate of decompression or H_2O content dissolved in the magma (e.g., Viccaro et al. 2010). After the dissolution incident, many crystals have got united as GLO, which successively re-grew as a single grain; however, others have re-grown through mantling on CS cores (crystals born after the decompression events as they represent smaller and medium size phenocrysts) and are devoid of CS morphology.

The shallow chamber was dynamically active because of the convection phenomenon, the input of new magma pulses, or the combination of both (Fig 25). Accordingly, by the heterogeneous superheating and convection processes, the growth of both pre-existing and newly brought crystals was constrained. Thus, they developed FS, FOZ, RS, and SY micro-textures. The repeated occurrence of FS in a single grain indicates the occurrence of the multiple superheating events. Moreover, during magma mixing superheating can also occur (Tsuchiyama 1985). Therefore, it can be stated that FS is the product of superheating by recharge occurrence. Such recharge events could be similar to a cryptic-mixing process, in which the shallow chamber magma experiences frequent addition of small pulses of primitive and hotter magma of similar composition while being different in fugacity H_2O contents (e.g., Humphreys et al. 2006). Whenever the recharge event brought new pulses of primitive magma, the pre-existed crystals in the shallow chamber interacted, leading to the partial dissolution in the form of FS morphology. Following each partial dissolution, they were re-equilibrated with new Ca-rich magma and re-grown as An-rich plagioclase. This result can be explained by the anorthite jump observed within or just after FS domain. However, in the case of a profound change in magmatic parameters by a recharge event, the crystals experienced intense dissolution, which highlights the major RS to equilibrate with more primitive magma.

Beside the superheating, crystals in the shallow chamber also have undergone repeated movement across the magmatic gradients by convection or turbulence as evidenced by the FOZ domains and SY in plagioclase (e.g., Singer et al. 1995; Ginibre et al. 2002). Hence, the evidence such as FS, FOZ, and SY demonstrate that at the shallow chamber, crystals undergo a frequent dissolution-regrowth process in a convective recycling magmatic environment (Fig 25). It has to be noted that magma during the self-mixing process chamber might have undergone undercooling by degassing or water exsolution after violent aerial eruption producing MIC, BC, and ST crystals.

7. Conclusion

Various growth and morphological micro-textures in plagioclases and the change trend of their chemical composition were systematically investigated in volcanic rocks of East-SVC, eastern Iran. The formation of growth micro-textures (i.e., coarse/fine-sieve, fine-scale oscillatory zoning and resorption surfaces) in plagioclases of East-SVC volcanic rocks is not related to the changes of chemical composition of magma; rather, they can be associated with temperature variations, H_2O fugacity, and recharge event in the magma chamber. Besides, the occurrence of these changes can be associated with the self-mixing process in the magma chamber. This process in the magma chamber with recharge event could be the reason for the dynamic actions in the magma. Moreover, this process makes the morphological micro-textures (i.e., Glomerocryst, Synneusis, Swallow-tailed, Broken crystals, and Microlite) in the volcanic rocks in East-SVC. Plagioclases with intact crystal micro-textures are formed in the magma chamber after temperature and chemical composition changes. Final crystallization of magma (i.e., microlite plagioclases), was andesine, orthoclase, and bytownite; therefore, the recharge of basic magma at the base of the magma chamber did not change completely the chemical composition on the magmatic system.

In addition, the changes trend of Fe, Mg, Ti, and Ca elements in clinopyroxene of andesite rocks East-SVC is very limited. Such changes could be related to the recharge of basic magma at the base of the magma chamber. Thermobarometry by using pyroxene and biotite chemistry showed that the temperature ranges for volcanic rocks of East-SVC were between 700 and 1150°C and the pressure was less than 2 kbar. Such variations can be related to the deeper depth of magmatic environment with respect to the shallow magmatic chamber.

Acknowledgement

This paper is supported financially by the Research Office of the Payam Noor University. The authors would like to thank the anonymous reviewers for their valuable comments and suggestions to improve the quality of the paper.

References

Abdel-Rahman A (1994) Nature of biotites from alkaline, calc-alkaline and peraluminous magmas, *Journal of Petrology* 35: 525– 541.

Angiboust S, Agard P, De Hoog JCM, Omrani J, Plunder A (2013) Insights on deep, accretionary subduction processes fromthe Sistan ophiolitic "melange" (Eastern Iran), *Lithos* 156: 139–158.

Arjmandzadeh R, Karimpour MH, Mazaheri SA, Santos JF, Medina JM, Homam SM, (2011) Sr/Nd isotope geochemistry and petrogenesis of the Chah-Shaljami granitoids (Lut Block, Eastern Iran), *Journal of Asian Earth Sciences* 41: 283–296.

Babazadeh SA, de Wever P (2004) Early Cretaceous radiolarian assemblages from radiolarites in the Sistan Suture (eastern Iran), *Geodiversitas* 26:185–206.

Beccaluva L, Macciotta G, Piccardo GB, Zeda O (1989) Clinopyroxene composition of ophiolite basalts as petrogenetic indicator, *Chemical Geology* 77:165-182.

Bröcker M, Fotoohi Rad G, Burgess R, Theunissen S, Paderin I, Rodionov N, Salimi Z (2013) New age constraints for the geodynamic evolution of the Sistan Suture Zone, eastern Iran, *Lithos* 170–171: 17–34.

Camp VE, Griffis RJ (1982) Character, genesis and tectonic setting of igneous rocks in the Sistan suture zone, eastern Iran, *Lithos* 15: 221–239.

Couch SR, Sparks SJ, Carroll MR (2001) Mineral disequilibrium in lavas explained by convective self-mixing in open magma chambers, *Nature* 411: 1037-1039.

Deer WA, Howie RA, Zussman J (1966) An introduction to the rock forming minerals, *UK: Longman Group UK Ltd* 528.

Elthon D (1987) Petrology of the gabbroic rocks from the Mid-Cayman rise spreading centre, *Journal of Geophysical Research* 92: 658–682.

Foster MD (1960) Layer charge relations in the dioctahedral and trioctahedral micas, *American Mineralogist* 45: 383-398.

Ginibre C, Kronz A, Wörner G (2002) High-resolution quantitative imaging of plagioclase composition using accumulated backscattered electron images: new constraints on oscillatory zoning, *Contributions to Mineralogy and Petrology* 142: 436-448.

Ginibre C, Wörner G, Kronz A (2007) Crystal zoning as an archive for magma evolution, *Mineralogical Society of America* 3(4): 261–266.

Henry DJ, Guidotti CV, Thomoson JA (2005) The Ti-saturation surface for low-to-medium pressure metapelitic biotites: implications for geothermonmetry and Ti-substitution mechanisms, *American Mineralogist* 90: 316-328.

Humphreys MCS, Blundy JD, Sparks SJ (2006) Magma evolution and opensystem processes at shiveluch volcano: insights from phenocryst zoning, *Journal of Petrology* 47 (12): 2303-2334.

Huppert HE, Sparks RS, Turner JS (1982) Effect of volatiles on mixing in calcalkaline magma systems, *Nature* 297: 554-557.

Kahl M, Chakraborty S, Pompilio M, Costa F (2015) Constraints on the nature and evolution of the magma plumbing system of mt. etna volcano (1991–2008) from a combined thermodynamic and kinetic modelling of the compositional record of minerals, *Journal of Petrology 56: 2025-2068.*

Karimpour MH, Malekzadeh Shafaroudi A, Farmer L, Stern CR (2012) Petrogenesis of Granitoids, U-Pb zircon geochronology, Sr-Nd Petrogenesis of granitoids, U-Pb zircon geochronology, Sr-Nd isotopic

characteristics, and important occurrence of Tertiary mineralization within the Lut block, eastern Iran, *Journal of Economic Geology* 4(1): 1-27 (in Persian with English abstract).

Karimpour MH, Stern CR, Farmer L, Saadat S, Malekezadeh A (2011) Review of age, Rb\Sr geochemistry and petrogenesis of Jurassic to Quaternary igneous rocks in Lut Block, Eastern Iran, *Geopersia* 1: 19–36.

Karsli O, Aydın F, Sadıklar MB (2004) Magma interaction recorded in plagioclase zoning in granitoid systems, Zigana Granitoid, eastern Pontides, Turkey, *Turkish Journal of Earth Sciences* 13: 287-305.

Le Base MJ (1962) The role of aluminum in igneous clinopyroxenes with relation to their Parentage, *American Journal of Science* 26: 267-288.

Leterrier J, Maury RC, Thonon P, Girard D, Marchal M (1982) Clinopyroxene composition as a method of identification of the magmatic affinities of paleo-volcanic series, *Earth and Planetary Science Letters* 59(1): 139-154.

Lindsley DH (1983) Pyroxene thermometry, *American Mineralogist* 68: 477-493.

Marsh BD (1998) On the interpretation of crystal size distributions in magmatic systems, *Journal of Petrology* 39 (4): 553-599.

Mazhari SA (2016) Geochemistry and petrogenesis of volcanic associations in Zouzan area, East of Iran, *Arabian Journal of Geosciences* 9: 37.

McCall GJH (1997) The geotectonic history of the Makran and adjacent areas of southern Iran, *Journal of Asian Earth Sciences* 15: 517–531.

Morimoto N (1989) Nomenclature of Pyroxenes, *Canadian Mineralogist* 27: 143-156.

Nachit H, Razafimahefa N, Stussi JM, Carron JP (1985) Composition chimique des biotites et typologie magmatique des granitoides, *Comptes Rendus de l'Académie des Sciences Paris* 301: 813-819.

Nazari H, Salamati R (1999) Geological map of Sarbisheh (1:100000), Sheet 7955, *Geological survey of Iran*.

Nisbet EG, Pearce JA (1977) Clinopyroxene composition in mafic lavas from different tectonic settings, *Contributions to Mineralogy and Petrology* 63: 149–160.

Pang KN, Chung SL, Zarrinkoub MH, Khatib MM, Mohammadi SS, Chiu HY, Chu CH, Lee HY, Lo CH (2013) Eocene–Oligocene post-collisional magmatism in the Lut–Sistan region, eastern Iran: Magma genesis and tectonic implications, *Lithos* 180–181: 234–251

Pang KN, Chung SL, Zarrinkoub MH, Mohammadi SS, Yang HM, Chu CH, Lee HY, Lo CH (2012) Age, geochemical characteristics and petrogenesis of Late Cenozoic intraplate alkali basalts in the Lut–Sistan region, eastern Iran, *Chemical Geology* 306–307: 40–53.

Pietranik A, Koepke J, Puziewicz J (2006) Crystallization and resorption in plutonic plagioclase: Implications on the evolution of granodiorite magma (Gesiniec granodiorite, Strzelin Crystalline Massif, SW Poland), *Lithos* 86: 260-280.

Renjith ML (2014) Micro-textures in plagioclase from 1994e1995 eruption, Barren Island Volcano: Evidence of dynamic magma plumbing system in the Andaman subduction zone, *Geoscience Frontiers* 5: 113-126.

Schroder JW (1944) Essai sur la structure de l'Iran, *Ecologae Geologicae Helvetiae* 37: 37–81.

Shabani AAT, Masoudi F, Tecce F (2010) An investigation on biotite composition from Mashhad granitoid rocks, NW Iran, *Journal of Science of Islamic Republic of Iran* 21: 321-331.

Singer BS, Dungan MA, Layn GD (1995) Textures and Sr, Ba, Mg, Fe, K, and Ti compositional profiles in volcanic plagioclase: clues to the dynamics of calcalkaline magma chambers, *American Mineralogist* 80: 776-798.

Smith VC, Blundy JD, Arce JL, (2009) Atemporal record of magma accumulation and evolution beneath Nevado de Toluca, Mexico, preserved in plagioclase phenocrysts, *Journal of Petrology* 50: 405-426.

Soesoo A (1997) A multivariate statistical analysis of clinopyroxene composition: empirical coordinates for the crystallisation PT-estimations, *Geological Society of Sweden (Geologiska Föreningen)* 119: 55-60.

Spear JA (1984) Micas in igneous rocks, In: Micas, Bailey, S.W., (ed); Mineralogical Society of America, *Review in Mineralogy* 13: 299-356.

Stone D (2000) Temperature and pressure variations in suites of Archean felsic plutonic rocks, Berens river area, northwest superior province, Ontario, Cananda, *The Canadian Mineralogist* 38: 455-470.

Tarabi (2018) The Study of Petrology of, Geochemistry and Alteration of Momen Abad Area (North_East of Sarbisheh) with Reference to the Formation of Bentonite Deposits and their Industrial Application, *PhD Thesis Islamic Azad University, Tehran Science and Research Branch* 345p (in Persian).

Tarabi S, Emami M, Modabberi S, Sheikh Zakariaee SJ (2019) Eocene-Oligocene volcanic units of momen abad, east of Iran: petrogenesis and magmatic evolution, *Iranian Journal of Earth Sciences* 11(2): 126-140.

Tirrul R, Bell IR, Griffis RJ, Camp VE (1983) The Sistan suture zone of eastern Iran, *Geological Society of America Bulletin* 94: 134–150.

Tsuchiyama A (1985) Dissolution kinetics of plagioclase in the melt of the system diopside-albite-anorthite, and origin of dusty plagioclase in andesites, *Contributions to Mineralogy and Petrology* 89 (1): 1-16.

Uchida E, Endo S, Makino M (2007) Relationship between solidification depth of granitic rocks and formation of hydrothermal ore deposits, *Resource Geology* 57: 47-56.

Verdel C, Wernicke BP, Hassanzadeh J, Guest B (2011) A Paleogene extensional arc flare-up in Iran, *Tectonics* 30 (TC3008):1-20.

Vernon RH, Johnson SE, Melis EA (2004) Emplacement-related microstructures in the margin of a deformed pluton:the San Jose´ tonalite, Baja California, Me´xico, *Journal of Structural Geology* 26: 1867–1884.

Viccaro M, Calcagno R, Garozzo I (2015) Continuous magma recharge at Mt. Etna during the 2011–2013 period controls the style of volcanic activity and compositions of erupted lavas, *Mineralogy and Petrology* 109: 67-83.

Viccaro M, Giacomoni PP, Ferlito C, Cristofolini R (2010) Dynamics of magma supply at Mt. Etna volcano (Southern Italy) as revealed by textural and compositional features of plagioclase phenocrysts, *Lithos* 116 (1-2): 77-91.

Waight TE, Maas R, Nicholls IA (2000) Fingerprinting feldspar phenocrysts using crystal isotopic composition stratigraphy: implications for crystal transfer and magma mingling in S-type granites, *Contributions to Mineralogy and Petrology* 139: 227–39.

Walker R, Gans P, Allen MB, Jackson J, Khatib M, Marsh N, Zarrinkoub M (2009) Late Cenozoic volcanism and rates of active faulting in eastern Iran, *Geophysical Journal International* 177: 783–805.

Walker R, Jackson J (2002) Offset and evolution of the Gowk fault, S.E. Iran: a major intra-continental strike-slip system, *Journal of Structural Geology* 24: 1677–1698.

Whitney DL, Evans BW (2010) Abbreviations for names of rock-forming minerals, *American Mineralogist* 95: 185–187.

Yazdi A, Ashja-Ardalan A, Emami MH, Dabiri R, Foudazi M (2017) Chemistry of Minerals and Geothermobarometry of Volcanic Rocks in the Region Located in Southeast of Bam, Kerman Province, *Open Journal of Geology* 7: 1644-1653.

Yazdi A, Shahhosini E, Dabiri R, Abedzadeh H (2019) Magmatic Differentiation Evidences And Source Characteristics Using Mineral Chemistry In The Torud Intrusion (Northern Iran), *Revista GeoAraguaia* 9(2): 6-21.

Yu H, Xu J, Lin C, Shi L, Chen X (2012) Magmatic processes inferred from chemical composition, texture and crystal size distribution of the Heikongshan lavas in the Tengchong volcanic field, SW China, *Journal of Asian Earth Sciences* 58: 1-15.

Zarrinkoub MH, Pang KN, Chung SL, Khatib MM, Mohammadi SS, Chiu HY, Lee HY (2012) Zircon U\Pb age and geochemical constraints on the origin of the Birjand ophiolite, Sistan suture zone, eastern Iran, *Lithos* 154: 392–405.